CTCF binding landscape is established by the epigenetic status of the nucleosome, well-positioned relative to CTCF motif orientation

Md Tajmul[1], Dharmendra Nath Bhatt[1], Luminita Ruje[2], Emma Price[1], Yon Ji[1], Dmitri Loukinov[1], Vladimir B. Teif[2], Victor V. Lobanenkov[1] and Elena M. Pugacheva[1]*.

[1] Molecular Pathology Section, Laboratory of Immunogenetics, Division of Intramural Research/ National Institute of Allergy and Infectious Diseases (NIAID)/ National Institutes of Health (NIH), Bethesda, MD 20892, USA

[2]School of Biological Sciences, University of Essex, Wivenhoe Park, Colchester CO4 3SQ, United Kingdom.

*Lead Contact. To whom correspondence may be addressed: Elena M. Pugacheva (epugacheva@niaid.nih.gov)

Abstract

CTCF binding sites serve as anchors for the 3D chromatin architecture in vertebrates. The functionality of these anchors is influenced by the residence time of CTCF on chromatin, which is determined by its binding affinity and its interactions with nucleosomes and other chromatin-associated factors. In this study, we demonstrate that CTCF occupancy is driven by CTCF motifs strategically positioned at the entry sites of a well-positioned nucleosome, such that, upon binding, the N-terminus of CTCF is oriented towards the nucleosome. We refer to this nucleosome as the CTCF priming nucleosome (CpN). CTCF recognizes its binding sites if they are not methylated. It can then displace the CpN, provided the nucleosome is not marked by CpG methylation or repressive histone modifications. Under these permissive conditions, the N-terminus of CTCF recruits SMARCA5 to reposition the CpN downstream, thereby creating nucleosome-free regions that enhance CTCF occupancy and cohesin stalling. In contrast, when CpNs carry repressive epigenetic marks, CTCF binding is transient, without nucleosome displacement or chromatin opening. In such cases, cohesin is not effectively retained at CTCF binding sites. We propose that the epigenetic status of CpNs governs cell-specific CTCF binding patterns, ensuring the maintenance of chromatin architecture throughout the cell cycle.

Graphical Abstract

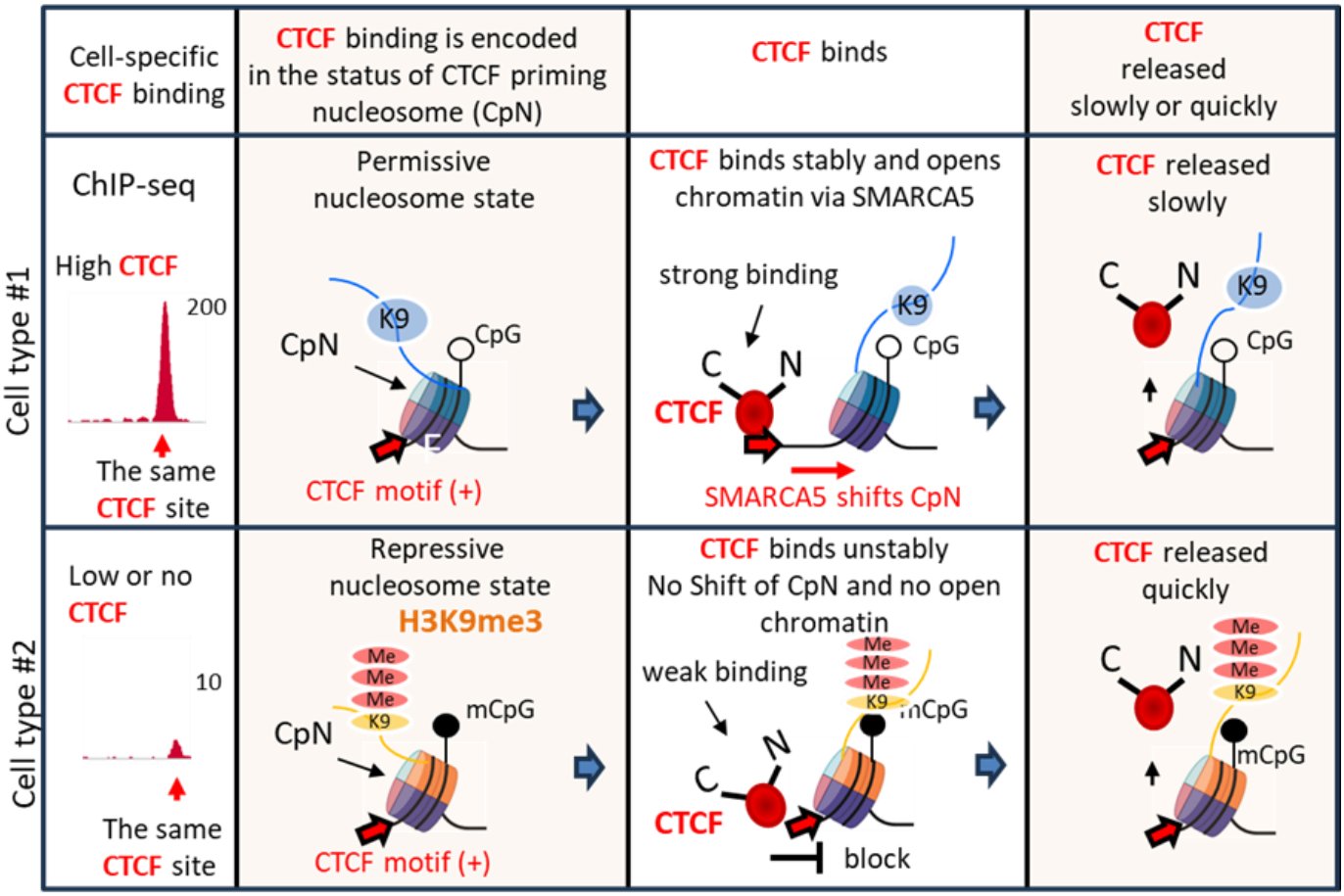

Introduction

3D genome organization in vertebrates is largely shaped by CTCF, which stops cohesin-guided extrusion of chromatin at its binding sites in the convergent orientation (1,2). CTCF is a ubiquitously expressed, highly conserved 11 Zinc Finger (ZF)-DNA binding factor (3). As part of the ENCODE project, CTCF binding sites were among the first to be mapped by ChIP-seq across multiple tissues and species (4). It is estimated that there are approximately 326,000 CTCF binding sites in the human genome, with an average of 66,000 sites occupied by CTCF in a single cell type (5). CTCF binding sites serve as anchors for 3D genome organization (2), activators or repressors of transcription (6), insulators (7), imprinting control regions (8), DNA repair sites (9), and more (10). Dysfunction of CTCF binding sites has been associated with various pathological conditions, including myotonic dystrophy (11), aberrant X-chromosome inactivation (12), neurodevelopmental disorders (13), and cancer (14,15).

Although the overall CTCF binding pattern remains largely consistent across different cell types, a small but significant proportion (~10-30%) of CTCF binding sites are cell type-specific (16). These cell-specific sites play a critical role in defining cell identity by contributing to cell-specific 3D genome organization and gene transcription (17). For instance, during ES cell differentiation into distinct lineages, changes in CTCF occupancy—marked by the loss and gain of cell-specific sites—are closely linked to cell specialization (18). Similarly, unique cancer-specific CTCF binding patterns have been identified across various human malignancies (14), and anti-cancer drug treatments have been shown to alter CTCF occupancy (19) (20). Therefore, CTCF binding patterns appear to be fundamental to cell fate and specialization. The dynamic reorganization of CTCF occupancy may represent a crucial cellular mechanism for adapting to new conditions or environmental challenges. Nevertheless, key questions remain underexplored: What determines the specificity of CTCF binding in different cell types, and how are changes in CTCF occupancy achieved during processes such as development, differentiation, or stress responses?

It has been established that CTCF occupancy is regulated by CpG methylation (21,22), cell-specific transcription factors (TFs) (17,23), kinases that phosphorylate ZFs to displace CTCF during mitosis (24) or in hormone response (25), chromatin remodeling factors that open chromatin for CTCF occupancy (26), histone marks (27) and more (28). CTCF binds a great assortment of DNA sequences using combinatorial clustering of its 11 ZFs (29) (30). CTCF ZFs

3-7 are responsible for recognition and binding the 15-bp CTCF core consensus (29), while ZFs 1-2 and ZFs 9-11 bind downstream and upstream from the core consensus sequences, respectively (31). CTCF bound sites are located in nucleosome-depleted regions (NDRs) flanked by several well-positioned nucleosomes around CTCF binding sites (32). Single-molecule level analysis of chromatin structure has demonstrated that only a small fraction of individual fibers is bound by CTCF at any given time in a cell population (33). Similar conclusions about the transience of CTCF binding were drawn from single-cell nucleosome positioning (34) and single-cell DNA-footprint (35). CTCF binding is dynamic, with CTCF protein binding on and off chromatin with an average residence time of 1-2 minutes (36,37). Such dynamic binding is essential for 3D genome organization and necessary for chromatin extrusion by cohesin (16). When CTCF is off chromatin, its place is occupied by a nucleosome (35,38,39). To re-bind to chromatin, CTCF must first reposition this nucleosome. This process involves chromatin-remodeling factors such as SNF2H (SMARCA5), CDH4, and BRG1, which can slide, evict, or remove nucleosomes around CTCF binding sites (26,40). Consequently, nucleosomes play a crucial role in regulating CTCF occupancy. Evidence supporting this includes the significant loss of CTCF occupancy observed after the loss of SMARCA5, which disrupts CTCF's ability to reposition nucleosomes and re-bind to its target sites (26,41,42).

The CTCF-nucleosome regulation model suggests that CTCF can recognize and bind to its sites even when they are occupied by nucleosomes (35). Moreover, CTCF restores the exact same binding pattern in daughter cells after mitosis, during which most CTCF is released from chromatin due to phosphorylation of CTCF zinc fingers (24,43). Additionally, when CTCF is degraded using auxin-degron systems, its occupancy is erased, but upon auxin removal, CTCF occupancy is restored exactly as it was before (44). These observations suggest that the CTCF binding pattern for each cell type is encoded in the DNA and chromatin status, thereby maintaining cell identity.

In this study, we sought to identify how chromatin status is involved in a cell-specific CTCF occupancy. By comparing ChIP-seq and Affinity-seq data from the same cell type, we analyzed CTCF binding sites both *in vivo* and *in vitro*. Based on our findings, we propose a model for the regulation of CTCF occupancy that is driven by the epigenetic status of the nucleosome that is well-positioned relative to CTCF binding sites. To confirm this proposed model, we used wild type (wt) and mutant (mut) CH12 cells. Compared to wtCH12 cells, a homozygous deletion of

CTCF ZF 9-11 in mutCH12 cells resulted in a loss of CTCF occupancy at five thousand (5K) binding sites (45,46). Ectopic expression of wild type CTCF in the mutCH12 cells not only recapitulated CTCF occupancy like in wild type cells but, most importantly, restored CTCF occupancy at the same 5K lost CTCF sites (45), suggesting that these sites are somehow pre-marked to be bound by CTCF in the CH12 cells. In this study, we demonstrate that cell-specific CTCF occupancy is preprogrammed not only by the status of CpG methylation in the CTCF site itself, but also by the status of CpG methylation and histone modifications of the nucleosome asymmetrically positioned relative to CTCF binding site.

Materials and methods

Cell culture, plasmids.

CH12 wild type (wt) and mutant (mut) cells were described previously in (45,46) and obtained as a gift from Dr. Casellas's lab. The cell lines were maintained in RPMI 1640 supplemented with 10% FBS, 1% penicillin/streptomycin and 55 μM 2-β mercaptoethanol. All ectopically expressed CTCF and BORIS constructs described in this study were designed on a backbone of pMy-MouseCTCFbiotag-T2A-mOrange plasmid (Addgene plasmid #50564) and described in (45). NIH3T3, stably expressing either EV (Empty Vector) or BORIS (clone#2), were maintained in Dulbecco's modified Eagle's medium (DMEM) supplemented with 10% of fetal calf serum and penicillin–streptomycin, described in (23).

ChIP-seq.

For ChIP-seq, $2x10^6$ asynchronously growing cells were crosslinked with 1% formaldehyde for 10 minutes at room temperature, followed by quenching with 125 mM glycine for 10 minutes. Cells were then washed twice with 1× phosphate-buffered saline (PBS) and resuspended in chromatin immunoprecipitation (ChIP) lysis buffer (150 mM NaCl, 1% Triton X-100, 0.1% SDS, 20 mM Tris-HCl pH 8.0, 2 mM EDTA). Chromatin was sheared to 200–600 bp and immunoprecipitated using 5 μg of respective antibodies. The immunoprecipitated DNA was purified using Zymo-spin™ columns (ZymoResearch), and DNA concentration was measured with a Qubit 4 Fluorometer (ThermoFisher). For sequencing, 5–10 ng of DNA was used to prepare libraries with the NEBNext Ultra II DNA Library Prep Kit for Illumina (New England, Catalog E7645S). Paired-end sequencing was performed on a NovaSeq 6000 system. All ChIP-seq experiments were conducted with at least two biological and/or technical replicates. Antibodies used in ChIP-seq: SMARCA5 (Snf2h) (Abcam, #ab3749), H3K9me3 (Abcam, ab#8898), RAD21 (Abcam, ab217678), SMC3 (Abcam, ab#9263), SMC1 (Bethyl Laboratories, #A300-055A).

ATAC-seq.

Freshly growing CH12 cells (5×10^4) were pelleted by centrifugation and resuspended in 50 μL of cold lysis buffer (10 mM Tris-HCl, pH 7.4, 10 mM NaCl, 3 mM $MgCl_2$, 0.1% IGEPAL CA-630), gently pipetting up and down ten times. Nuclei were pelleted by centrifugation at 2500g for

10 min at 4°C and resuspended in 25 µL of 2x TD Buffer (Illumina Cat #FC-121-1030), containing 8 µL of Tn5 Transposes (Illumina Cat #FC-121-1030) and 17 µL of nuclease-free water. The reaction was incubated for 30 min at 37°C. Tagmented DNA was purified by using a Zymo Research DNA Clean & Concentrator™-5 - Capped Columns. The libraries were amplified using NEBNext High-Fidelity 2× PCR Master Mix (New England Biolabs, M0541). The libraries were size-selected by adding 1.8X volume Agencourt AMPure XP beads (Beckman, 63881). Library concentration was measured by DNA High Sensitivity Kit (Invitrogen) on a Qubit fluorometer (Invitrogen). Library quality and fragment sizes were assessed on a Bioanalyzer (Agilent). ATAC-Seq libraries from at least two biological replicates for each condition were paired-end-sequenced on an Illumina NextSeq550 platform. ATAC-seq libraries were generated as previously described (47).

MNase-Seq Assisted H3 ChIP-seq.

MNase-ChIP-seq was performed on wtCH12 or mutCH12 fixed cells using the SimpleChIP® Enzymatic Chromatin IP Kit (Magnetic Beads) (Cell Signaling Technology, Cat #9003) following the manufacturer's protocol. Briefly, after obtaining MNase-digested lysates as described in the MNase-seq method, chromatin lysates were incubated with 5 µg of Histone H3 (Cell Signaling, #D2B12) XP® Rabbit mAb and rotated overnight at 4°C. Following this incubation, 30 µL of Protein G Magnetic Beads were added to the mixture and rotated for 2 hours at 4°C. The Protein G magnetic beads were then pelleted using a magnetic separation rack for 1–2 minutes. The supernatant was carefully removed, and the beads were washed three times with 1 mL of low salt wash buffer, incubating each wash for 5 minutes at 4°C with rotation. After the final low salt wash, 1 mL of high salt wash buffer was added, and the beads were incubated again for 5 minutes at 4°C with rotation. The beads were pelleted, and the supernatant was removed. Next, 150 µL of 1X ChIP Elution Buffer was added, and the chromatin was eluted from the antibody/Protein G magnetic beads by placing the tubes on a thermomixer at 65°C for 30 minutes with gentle shaking (1,000 rpm). The eluted chromatin supernatant was transferred to a new tube, and the immunoprecipitated DNA was purified according to the kit protocol. Sequencing libraries were prepared using the NEBNext® Ultra™ II DNA Library Prep Kit (New England, Catalog E7645S).

MeDIP Library Preparation.

Genomic DNA (gDNA) was extracted from freshly growing CH12 cells and sonicated using a Covaris ultrasonicator to obtain a mean fragment size of 200 bp. For library preparation, 5 μg of sonicated gDNA was end-repaired and ligated with adaptors using the NEBNext Ultra DNA Library Prep Kit for Illumina (New England, Catalog E7645S). The reaction mixture was then purified with AMPure XP beads (Beckman-Coulter, CA, USA, Catalog #A63881). For precise size selection, half of the sample was run on a 1.5% agarose gel, and DNA fragments of 150-250 bp were extracted from the gel. Both the size-selected and non-size-selected libraries were denatured at 95°C for 10 minutes, followed by incubation on ice for 10 minutes. The denatured DNA was subjected to immunoprecipitation with 5-Methylcytosine antibody (Active Motif, Catalog #61479) by incubating the reaction mixture at 4°C for 15 hours. The immunoprecipitated DNA was size-selected again using AMPure XP beads and amplified using Q5 High-Fidelity DNA Polymerase (New England Biolabs, Catalog #M0491). The amplification products were purified with AMPure XP beads. Finally, the purity and fragment length distribution were assessed using a Bioanalyzer 2100 (Agilent Technologies), and the libraries were subjected to deep sequencing on the Illumina HiSeq 2000 platform.

Published Next-Generation Sequencing (NGS) datasets used in this study.

For the Affinity-seq mouse spleen data, we used the dataset GSE111772, generated in (48). For CTCF ChIP-seq, we used the following datasets: mouse spleen GSM918745 (49); CH12 cells (GSE137216), mouse ES cells (SRR5085156, SRR5085157), NIH3T3 cells (GSE207058), MCF7 cells (GSE70764), K562 cells (GSE137216). For RAD21 ChIP-seq, we used the following datasets: CH12 cells (GSE137216), NIH3T3 (current study), mES cells (SRR5085154, SRR5085155). To generate Figure 1D, 1E and Supplementary Figures S2, S6 we used the genomic coordinates (in the mouse genome version mm9) provided in Table S1, along with the following NGS data for CH12 cells: MNAse-H3 ChIP-seq (current study), H3K9me3 ChIP-seq (GSM918745) from (49), and 5mC MeDIP-seq (GSM1368909) from (50). To generate Supplementary Figures S3 and S4, we used the following NGS data for mES cells: H3K9me3 (SRR566935), MNase-H3 (GSE146082), 5mC MeDIP-seq (SRR6321573). To generate Supplementary Figure S5, we used H3K9me3 ChIP-seq for mouse spleen (SRR21231093). To generate Supplementary Figures S7 and S8, we used the following NGS data: for MCF7 cells: MNase-seq (SRR3142031, SRR3142029), H3K9me3 ChIP-seq (SRR21231093), 5mC MeDIP-

seq (SRR12358951); for K562 cells: MNase-seq (SRR3211681, SRR3211680), 5mC MeDIP-seq (SRR1237957). For Figure 5 and Supplementary Figure S9, we used datasets from (26), for SMARCA5 knockout in Kasumi-1 cells (GSE220778, GSE160470, GSE160469) (26). To extract CTCF motifs bound by CTCF in Kasumi-1 cells, we used CTCF ChIP-seq from SRR8060948. For ATAC-seq data we used the following NGS data: mouse ES cells (SRR14701291) (51), NIH3T3 (GSE207058) (23), CH12 cells (current study). For wtCH12 and mutCH12 cells, we utilized ChIP-seq dataset GSE137216 (for CTCF, BORIS, FL-CTCF, deltaC-CTCF, and deltaN-CTCF), which were generated in our previous study (45). For NIH3T3 cells, we used ChIP-seq dataset GSE207058 that we previously generated by our lab (23).

Bioinformatic analysis of ChIP-seq, ATAC-seq, MNase-seq, meDIP-seq data.

Sequences generated by the Illumina or NovaSeq 6000 were aligned against either the human (build hg19) or mouse (build mm9) genome using the Bowtie2 program with options "–very-sensitive -X 2000" (52). Bowtie output files (SAM) were converted into BAM files using the "samtools view" option in SAMtools (53), and these BAM files were then used for generating heatmaps with DeepTools (54). To call ChIP-seq or meDIP-seq peaks we applied MACS2 peak calling algorithm with defaults parameters (55). The ChIP-seq data were visualized using the Integrative Genomics Viewer (IGV) (56). The peak overlaps between ChIP-seq data sets were determined with the BEDTools Suite, with at least 1 bp overlap (57). For ATAC-seq, the open chromatin regions were called using MACS2 with options: –nomodel – shift -100 – extsize 200 -f BAMPE. For MNase-Seq Assisted H3 ChIP-seq, we produced multiple replicates that exhibited a strong Pearson correlation, typically ranging from 0.75 to 0.95, ensuring robust reproducibility. The best replicates were combined into one set for heatmap visualization using DeepTools.

Affinity-Seq data.

CTCF Affinity-seq data for 3-month-old mouse spleen were generated in the Zuo et al. study (48). In this study, the authors isolated genomic DNA from mouse spleen using the phenol-chloroform extraction method and randomly sheared it to ∼200 bp fragments through sonication (48). This extraction method preserves the DNA CpG methylation status, allowing mapping of CTCF binding only to unmethylated DNA sequences. The genomic DNA was incubated overnight with purified

6HisHALO-tagged CTCF 11-Zinc fingers protein (48). In the current study, we downloaded the FASTQ files for CTCF Affinity-seq data from mouse spleen (GSM3039567) and mouse control DNA (GSM3039568) from the series GSE111772. The FASTQ files were aligned to the mouse genome (mm9 build) using Bowtie2 with the options "–very-sensitive -X 2000." The resulting Bowtie output files (SAM) were converted into BAM files, which were subsequently used for generating heatmaps with DeepTools. To call peaks for Affinity-seq, we applied the MACS2 peak-calling algorithm with default parameters, using mouse control DNA as the input control. The list of Affinity-seq CTCF peaks is provided in Supplementary Table 1.

Heatmaps for NGS data visualization.

The heatmaps of ChIP-Seq, ATAC-seq, MeDIP-seq, MNase-seq-H3 ChIP tag densities for different clusters were generated using DeepTools (54). For heatmap visualization of ATAC-seq data, we sorted BAM files of paired-end mapped reads into two categories based on fragment size, using the bamCoverage option from DeepTools. For CTCF footprints, we applied the arguments "--Mnase --minFragmentLength 40 --maxFragmentLength 130", and for nucleosome positioning, we used "--Mnase --minFragmentLength 160 --maxFragmentLength 200". For heatmap visualization of MNase-assisted H3 ChIP-seq data, we similarly used the bamCoverage option with the --Mnase argument. For ChIP-seq and meDIP-seq, we used just bamCoverage option without an additional argument. All BAM files in this study were normalized using the DeepTools option "--normalizeUsing RPKM". Heatmaps were generated using computeMatrix option to simultaneously visualize multiple NGS datasets at the same genomic coordinates. Since some datasets, like ChIP-seq, showed much higher enrichment values compared to MNase-H3 ChIP-seq or MeDIP-seq, we used plotHeatmap with different --zMax values to adjust the heatmap intensities. The heatmaps, each with different zMax values as reflected by the numbers on the average plots and scale bars, were then combined into a single figure.

Identification of CTCF binding motifs/consensuses.

For CTCF motif analysis, we used the summit CTCF ChIP-seq or CTCF Affinity-Seq BED files generated by MACS2. The sequences around the summits of ChIP-seq or Affinity-Seq peaks were extended by 50 bp upstream and downstream for CTCF motif discovery. FASTA files were

generated using BEDTools (getfasta option) based on either the human (hg19) or mouse (mm9) genome. These FASTA files were then used to recover position weight matrices using Multiple EM for Motif Elicitation (MEME) software (58). We ran MEME with the parameters (-nmotifs 1 -mod oops -revcomp -w 15, or -w20, or -w40) to identify the motif for CTCF ChIP-seq or CTCF Affinity-seq peaks. To determine the orientation of CTCF motifs for each CTCF ChIP-seq peak, we used the FIMO tool from the MEME suite with default settings (p-value < 0.0001). FIMO allowed us to identify the genomic coordinates and strand-specific CTCF motif orientation under each ChIP-seq peak called by MACS2. Based on the strand-specific orientation, CTCF motifs were classified as either plus or minus motifs for further analysis. In cases where the 100 bp window around the summit of a CTCF peak contained more than one CTCF motif, we selected the motif with the most significant p-value. If several motifs within a single CTCF ChIP-seq peak had identical p-values, those sites were excluded from the analysis. The list of plus and minus CTCF motifs used in this study is provided in Table S1. To calculate the total number of CTCF motifs in the mouse genome, we used the position weight matrices from CTCF ChIP-seq data in CH12 cells to scan the mouse genome (mm9) using the FIMO tool with default settings (p-value < 0.0001).

Results

About sixfold discrepancy between in vivo bound and potentially available CTCF binding sites

We initiated this study by asking how does the status of chromatin influence cell-specific CTCF occupancy. One of the most straightforward ways to address this question is to compare CTCF binding to chromatin with CTCF binding to naked DNA isolated from the same type of cells. This comparison provides information on how many sites are available for CTCF binding on DNA and how many are indeed bound in chromatin.

To this end, we used previously published studies (48,49) to compare CTCF binding sites in mouse spleen identified by either ChIP-seq (chromatin) or Affinity-seq (naked genomic DNA), using either CTCF antibodies or the 11 Zinc Finger DNA-binding domain of CTCF, respectively (Figure 1A). Using these two genome-wide approaches, we mapped 31,407 CTCF binding sites in chromatin and 191,231 potential CTCF binding sites in naked genomic DNA of mouse spleen,

respectively. (Figure 1A-B). The majority of CTCF sites (88%) bound *in vivo* (chromatin) were also identified by the 11 ZFs binding to naked genomic DNA (*in vitro*), confirming that the CTCF binding domain is a main factor of CTCF occupancy (Figure 1B).

However, there were 163,692 potential CTCF binding sites that were not occupied by CTCF *in vivo* while being accessible to the 11 ZFs domain binding based on Affinity-seq. Since Affinity-seq preserves genomic CpG methylation, which is known to negatively affect CTCF binding (21), DNA methylation alone cannot fully explain the absence of CTCF occupancy at these sites. Given that these sites were free of CpG methylation and available for 11 ZF binding, we hypothesized that other regulatory factors may influence CTCF occupancy *in vivo*. Interestingly, the comparison of ChIP-seq versus Affinity-seq showed that CTCF binding affinity is more consistent with the 11 ZFs domain binding to genomic DNA compared to the more variable CTCF binding to chromatin, confirming that different chromatin-environment factors influence CTCF occupancy *in vivo* (Supplementary Figure S1A).

Motif analysis of CTCF binding sites detected by ChIP-seq and Affinity-seq identified the classic 15-bp CTCF core consensus motif at the summit of the recovered peaks (Figure 1B). However, this motif alone is not sufficient to predict CTCF occupancy. When the mouse genome (mm9) was scanned for the 15-bp CTCF consensus, over 900,000 potential CTCF binding sites were detected, most of which were never bound by CTCF in the spleen or any other mouse cell types (Figure 1C and Supplementary Figure S1B). Interestingly, there were 3,868 CTCF ChIP-seq peaks in the mouse spleen that were not recovered by Affinity-seq. These CTCF peaks lacked the presence of the CTCF consensus motif, suggesting that CTCF may be able to bind to chromatin in unconventional ways (Figure 1B).

Thus, this analysis indicates that neither the presence of the CTCF consensus motif nor the absence of CpG methylation is fully sufficient to explain the cell-specific occupancy of CTCF *in vivo*.

CTCF motifs are strategically positioned at the entry sites of well-positioned nucleosomes, such that upon binding, the N-terminus of CTCF is oriented towards the nucleosome

Based on the comparison of ChIP-seq and Affinity-seq data (Figure 1B), it appears there are potentially six times more available CTCF binding sites than those actually bound by CTCF in

mouse spleen chromatin. Importantly, CTCF ChIP-seq data from various mouse tissues (ENCODE data) show that these potential binding sites are occupied by CTCF in other cell types (Figure 1C and Supplementary Figure S1B,C). This suggests that these sites are valid CTCF binding sites, likely free from CpG methylation (due to their accessibility to the 11 ZFs of CTCF), but exhibit tissue-specific chromatin properties that restrict CTCF binding in the spleen. We aim to investigate which DNA and chromatin features that render these potential CTCF sites unavailable for binding in the spleen while allowing CTCF binding in other cell types.

In Figure 1C, a genome browser visualization demonstrates that the potential CTCF binding sites recovered by Affinity-seq, but not by ChIP-seq in mouse spleen, are bound by CTCF in mouse B-cell lymphoma (CH12) and mouse embryonic stem (mES) cells (shown by arrows). There are also Affinity-seq recovered CTCF sites that are not bound by CTCF in CH12 and mES cells but bound by CTCF in other cell lines (Supplementary Figure S1B, C). Based on these observations, for future analysis, we categorized CTCF binding sites into three groups: (Group #1) sites bound by CTCF in the chromatin of the analyzed cells (CTCF-bound, ChIP-seq), (Group #2) Affinity-seq recovered sites not bound by CTCF in the chromatin of the analyzed cells (11 ZFs-only, naked DNA), and (Group #3) CTCF consensus sequences that are never bound by CTCF *in vivo* and not recovered by Affinity-seq (CTCF motif, not bound by CTCF) (Figure 1C). For each group, we randomly selected approximately 32,000 CTCF binding sites and divided them into plus (sense) and minus (antisense) CTCF consensus orientations, with 16,000 sites in each orientation (Figure 1D and Supplementary Figures S2-S4).

Previous studies have shown that CTCF competes with nucleosomes for DNA binding *in vivo* (35,38,39). Once bound to chromatin, CTCF can position nucleosomes on either side of its binding site (32). To investigate nucleosome positioning at the three selected groups of CTCF binding sites, we analyzed MNase-assisted H3 ChIP-seq data for both CH12 and mES cells (Figure 1D and Supplementary Figures S2-S4). We first examined plus-oriented CTCF consensus sites bound by CTCF in CH12 cells (Group #1) (Figure 1D, E). The combined analysis of CTCF occupancy via ChIP-seq and Affinity-seq, alongside nucleosome positioning, revealed distinct patterns related to nucleosome presence. High-occupancy CTCF ChIP-seq peaks were predominantly located in nucleosome-free regions, with well-positioned nucleosomes flanking the CTCF-bound sites. In contrast, low-occupancy CTCF sites were characterized by less frequent CTCF binding, and a

nucleosome approaching from the right side of plus-oriented CTCF consensus sites was more commonly detected (indicated by the blue arrow in Figure 1D). Interestingly, the same approaching nucleosome is well-positioned at Affinity-seq derived CTCF binding sites that are not bound by CTCF in CH12 cells (Group #2) (Figure 1D, E, blue arrow). This nucleosome is positioned such that, once CTCF binds, its N-terminus is oriented towards the nucleosome (31), with the CTCF consensus sequence located at the entry site of the nucleosome (Figure 1D, E). We refer to this nucleosome as the CTCF priming Nucleosome (CpN). For minus-oriented CTCF consensus sites, the CpN nucleosome is positioned on the left, with the N-terminus of CTCF facing towards it upon binding (Supplementary Figure S2, shown by blue arrow). The same analysis in mES cells showed consistent results with those observed in CH12 cells (Supplementary Figures S3-S4), indicating that the positioning of the CpN may play a role in regulating CTCF occupancy across cell types.

Based on these observations, we propose that CTCF binding sites are strategically positioned at the entry side of the CpN. At sites where CTCF strongly binds, it displaces the CpN for stable DNA binding, with its N-terminus oriented toward the nucleosome, shifting the nucleosome downstream from the binding site (Figure 1E, schematic, black arrow). In contrast, at sites identified only by Affinity-seq, CTCF is unable to displace the CpN for a strong DNA binding (Figure 1D, E and Supplementary Figures S2-S4). Therefore, we suggest that specific epigenetic features of the CpN may regulate CTCF's ability to bind in chromatin.

CTCF cannot successfully displace the priming nucleosome if the nucleosome carries the repressive histone mark H3K9me3 or is wrapped in a CpG-methylated sequence

Our next aim was to determine which epigenetic features may influence CTCF's ability to displace the nucleosome at CTCF-bound sites (as identified by ChIP-seq), but not at sites derived by Affinity-seq, which are not actually bound by CTCF *in vivo*. To investigate this, we analyzed two factors known to inhibit CTCF binding *in vivo*: the repressive histone mark H3K9me3 (via ChIP-seq) and genome-wide CpG methylation (assessed using MeDIP-seq with 5mC antibodies).

Our analysis of H3K9me3 ChIP-seq data in both CH12 and mES cells revealed that the CpN is enriched with the repressive histone mark at CTCF sites not bound by CTCF in the analyzed cells (11ZFs-only, Group#2) and at low-occupancy CTCF binding sites within the CTCF-bound Group #1. Conversely, high-occupancy CTCF bound sites are entirely depleted of H3K9me3 (Figure 1D

and Supplementary Figures S2A, S3-S4). Thus, we propose that the CpN, marked by the repressive histone modification H3K9me3, impedes CTCF's ability to effectively displace the nucleosome for a strong DNA binding. To test this hypothesis, we examined whether CTCF sites identified by Affinity-seq in spleen cells but not bound by CTCF *in vivo* could be attributed to the enrichment of H3K9me3 at the CpN. Our analysis of H3K9me3 ChIP-seq data in mouse spleen confirmed this hypothesis: the CpN of CTCF sites that were not occupied *in vivo* showed obvious enrichment of repressive histone marks, whereas these marks were absent from the CpN of CTCF-bound sites (Supplementary Figure S5). This finding corroborates our observations in CH12 and mES cells (Figure 1D and Supplementary Figures S2-S4), reinforcing the idea that the presence of H3K9me3 at the CpN is one of the key factors preventing strong CTCF binding *in vivo*.

The analysis of CpG methylation in CH12 cells at the three groups of selected CTCF sites showed that CTCF-bound sites (Group #1) were associated not only with the absence of CpG methylation at the CTCF consensus itself but also at the DNA sequence wrapped around the CpN (Figure 1D and Supplementary Figures S2A, S3). Thus, the methylation status of DNA wrapped around the CpN is also important for CTCF occupancy. In contrast, CTCF sites recovered by Affinity-seq only (Group #2) but not bound *in vivo* showed enrichment of CpG methylation precisely at the CpN, thus preventing a strong CTCF occupancy *in vivo* (Figure 1D and Supplementary Figure S2A). Group #3, consisting of CTCF sites never bound by CTCF, showed more widespread enrichment of both H3K9me3 and CpG methylation outside of the CpN (Figure 1D and Supplementary Figure S2A). Similar patterns were observed in mES cells, leading to the same conclusions (Supplementary Figures S3-S4).

Additionally, the analysis of CTCF binding sites specific to either CH12 or mES cells revealed that the presence of H3K9me3 and CpG methylation at the CpN inhibits or reduces CTCF binding in a cell-specific manner (Supplementary Figure S6). For example, CTCF sites that are bound only in mES cells are enriched with both H3K9me3 and CpG methylation in CH12 cells, suggesting a repressive environment that blocks CTCF binding. Conversely, CTCF sites bound only in CH12 cells are depleted of these repressive marks, allowing for strong CTCF binding in these regions (Supplementary Figure S6). Similar patterns were observed in the human cell lines K562 and MCF7, further supporting the idea that the cell-specific occupancy of CTCF is influenced by the epigenetic landscape surrounding the CpN (Supplementary Figure S7).

Notably, upon examining the genome browser views of CTCF ChIP-seq data across multiple cell lines (Figure 1C) and the heatmaps generated in this study, we observed that low-occupancy, small CTCF ChIP-seq peaks, those not classified as significant peaks by the MACS algorithm, but were recovered by Affinity-seq as strong CTCF binding sites. Furthermore, these peaks are also identified as cell-specific CTCF binding sites in other cell types, where they display high CTCF occupancy. This low CTCF occupancy is indicated by yellow arrows in Figure 1D and Supplementary Figures S1B,C, S2A, S3, S5, S6, S7C,D. Based on these observations, we suggest that there are many more CTCF binding sites in vertebrate cells than previously recognized. These sites may not be classified as significant ChIP-seq peaks but still bind CTCF briefly and specifically, provided that the CTCF consensus is not methylated. The repressive status of the CpN appears to protect these sites from stronger CTCF binding. The functionality of these sites remains an open question, but they do show a low enrichment of cohesin, suggesting their potential and brief involvement in 3D genome organization (Supplementary Figure S1C).

Based on the above observations, we propose that cell-specific CTCF occupancy is influenced by CTCF's ability to reposition the CpN for effective DNA binding. When the CpN is enriched with CpG methylation and/or H3K9me3 histone modifications, CTCF is less able to reposition the nucleosome, resulting in reduced or absent binding. Conversely, when the CpN lacks these modifications, CTCF can successfully displace the nucleosome, leading to stronger binding. Thus, both the methylation status and histone modification state of the CpN, as well as the CTCF binding site itself, are critical factors determining CTCF occupancy.

Cell-specific CTCF occupancy is pre-marked and stable within each cell type

Our findings outlined above suggest that cell-specific CTCF occupancy is established by the epigenetic status of the CpN. It is known that each cell type exhibits a unique pattern of CTCF occupancy, which plays a crucial role in 3D genome organization and the maintenance of cell identity (59). During mitosis, the majority of CTCF is released from chromatin, necessitating the re-establishment of the same CTCF binding pattern in daughter cells post-mitosis as was present in the mother cell (43). The use of auxin-degron systems to analyze CTCF dynamics has shown that, upon withdrawal of auxin, CTCF restores its binding pattern to its pre-depletion state (44). These observations suggest that cell-specific CTCF binding patterns are preprogrammed and preserved within the chromatin state of each cell type.

In this study, we sought to explore the mechanisms by which cell-specific CTCF occupancy is maintained and re-established, focusing particularly on the potential role of the CpN in pre-marking future CTCF binding sites. We hypothesized that the status of the CpN may serve as a memory marker for CTCF binding, preserving the specific occupancy pattern seen in each cell type across cell divisions. To test this hypothesis, we utilized a model system involving wild-type (wt) CH12 cells and mutant (mut) CH12 cells. The mutCH12 cells were previously generated through the homozygous deletion of CTCF zinc fingers (ZFs) 9-11, resulting in a truncated CTCF protein (Figure 2A, schematic) (46). This modification leads to the loss of mutant CTCF binding at approximately 5,000 (5K) CTCF sites in mutCH12 cells, as observed in comparative analyses of CTCF ChIP-seq data with wtCH12 cells (Figure 2B) and in (45). Previously, we demonstrated that ectopic expression of full-length (FL) CTCF in mutCH12 cells restores CTCF occupancy at these 5K lost sites, mirroring the pattern observed in wtCH12 cells (45) (Figure 2C,D). This suggests that these 5K sites hold inherent chromatin features that mark them for future CTCF occupancy, regardless of the loss of CTCF binding.

To investigate the chromatin features that mark these sites for CTCF binding, we also utilized various truncated forms of CTCF, lacking either the N-terminal (ΔN) or C-terminal (ΔC) regions, while retaining all 11 ZFs necessary for DNA binding to the 5K sites (Figure 2 C,D). This approach allowed us to dissect the roles of the C- and N-terminal domains of CTCF in the re-establishment of occupancy at the 5K sites. Furthermore, we explored the role of BORIS (CTCFL), a paralog of CTCF that shares a similar 11 ZF DNA-binding domain but differs in the C- and N-terminal regions (60,61). We previously showed that BORIS can bind to the 5K lost CTCF sites in mutCH12 cells, but not in wtCH12 cells, where it would normally compete with CTCF for binding (45).

To comprehensively analyze the chromatin and DNA features associated with these CTCF sites, we performed the following assays in wtCH12 and mutCH12 cells: ATAC-seq (to assess chromatin accessibility), MNase-seq (to map nucleosome positioning), MNase-assisted H3 ChIP-seq (to profile nucleosome occupancy), MeDIP-seq (to map DNA methylation), and H3K9me3 ChIP-seq (to identify repressive histone modifications). The use of wtCH12 and mutCH12 cells provides a unique system to investigate how the chromatin and DNA status changed with the loss of CTCF binding and the subsequent re-occupancy by CTCF and BORIS proteins (45).

Loss of CTCF occupancy results in the loss of chromatin accessibility, a state that cannot be restored at the CTCF binding sites without the N-terminus of CTCF

To investigate the changes in chromatin status following the loss of CTCF occupancy at the 5K CTCF sites in mutCH12 cells, we performed ATAC-seq analysis to compare chromatin accessibility in wtCH12 and mutCH12 cells. ATAC-seq using paired-end sequencing allowed us to categorize the reads into short fragments (<130bp), indicative of CTCF footprint, and nucleosome-sized fragments (>160bp) to determine nucleosome positioning (Figure 3). We analyzed chromatin accessibility at two groups of CTCF binding sites: 1). Remaining CTCF Sites (56K): these sites are bound by CTCF in both wtCH12 and mutCH12 cells and serve as a control; 2). Lost 5K CTCF Sites: these sites are bound by CTCF in wtCH12 cells but lose CTCF occupancy in mutCH12 cells (Figure 2B,C).

It is well-documented that CTCF bound sites are located in open chromatin regions with well-positioned nucleosomes flanking these sites (32). Our ATAC-seq analysis confirmed this at the remaining CTCF sites in both wtCH12 and mutCH12 cells, as well as at the 5K lost CTCF sites in wtCH12 cells, showing clear footprints of open chromatin and nucleosome positioning at the flank of CTCF sites (Figure 3A and Supplementary Figure S8B). However, in mutCH12 cells, the loss of CTCF occupancy at the 5K sites resulted in a complete loss of both open chromatin and nucleosome positioning around these sites (Figure 3B). This indicates that CTCF is crucial for maintaining an open chromatin state at its binding sites. Ectopic expression of FL-CTCF (tagged with V5-tag) in mutCH12 cells restored not only CTCF occupancy at the vast majority of the 5K lost sites (as mapped using V5-tag antibodies) but also reestablished open chromatin and nucleosome positioning around CTCF sites (Figure 3C). This restoration suggests that CTCF functions as a pioneer factor capable of binding and opening closed chromatin.

To determine which domain of CTCF is essential for chromatin opening and nucleosome repositioning, we expressed truncated versions of CTCF, tagged with V5, in mutCH12 cells. We found that truncations of either the C-terminus (deltaC) or the N-terminus (deltaN) led to less stable CTCF binding compared to FL-CTCF (Figure 1C-E and Supplementary Figure S8A). Importantly, CTCF lacking the C-terminus was still capable of opening chromatin and repositioning nucleosomes, but CTCF lacking the N-terminus was not (Figure 3D, E). This

demonstrates that the N-terminus of CTCF is essential for its ability to open chromatin and reposition nucleosomes. Unexpectedly, the N-terminus truncated version of CTCF was still able to bind the 5K lost CTCF sites without opening of chromatin (Figure 3E). Furthermore, we investigated the role of BORIS, a paralog of CTCF with a different N- and C-termini. Our analysis revealed that while BORIS could not open the chromatin at the 5K lost CTCF sites, it could still bind closed chromatin (as shown by BORIS ChIP-seq peaks) at the 5K sites in mut CH12 cells (Figure 3F). These data are corroborating previous findings regarding the N-terminus of CTCF and BORIS (62).

In conclusion, this analysis suggests that CTCF acts as a pioneer transcription factor capable of opening closed chromatin and repositioning nucleosomes. This pioneer activity is dependent on the N-terminus of CTCF, highlighting its critical role in chromatin dynamics and gene regulation.

Nucleosome positioning around CTCF binding sites depends on the N-terminus of CTCF

Our ATAC-seq data analysis demonstrated that CTCF-bound sites are associated with open chromatin and flanked by well-positioned nucleosomes, with these chromatin states being influenced by the N-terminus of CTCF (Figure 3). To validate the ATAC-seq findings, we performed micrococcal nuclease digestion followed by H3 histone ChIP sequencing (MNase-H3-ChIP-seq) to assess nucleosome status in wtCH12 versus mutCH12 cells. The MNase-H3-ChIP-seq analysis revealed that several well-positioned nucleosomes flank the remaining CTCF sites in both wtCH12 and mutCH12 cells, while the CTCF-bound sites themselves are depleted of nucleosome occupancy (Figure 4A and Supplementary Figure S8C). However, at the 5K lost CTCF sites in mutCH12 cells, the nucleosome positioning observed in wtCH12 cells was disrupted (Figure 4B) but restored with the ectopic expression of FL-CTCF in mutCH12 cells (Figure 4C).

Interestingly, in mutCH12 cells, we detected an enrichment of reads immunoprecipitated with H3 histone antibodies directly at the summit of the lost CTCF binding sites (Figure 4B, indicated by the red arrow). This enrichment likely corresponds to a single well-positioned nucleosome precisely at the CTCF binding site. By combining MNase-H3-ChIP-seq data at the 5K lost CTCF sites from both wtCH12 and mutCH12 cells, we confirmed that this nucleosome resides at the summit of the lost CTCF ChIP-seq peaks in mutCH12 cells, whereas the same regions are nucleosome-free in wtCH12 cells (Figure 4D).

Following our previous analysis in Figure 1D, we categorized the 5K lost sites into two groups based on the CTCF motif orientation. This categorization revealed the presence of the CpN at low occupancy CTCF binding sites in wtCH12 cells (Figure 4E, arrow). Moreover, upon the loss of the 10 well-positioned nucleosomes at the 5K sites in mutCH12 cells, the CpN became the only well-positioned nucleosome within a 2 kb window around the CTCF binding site (Figure 4D,E). Consistent with prior Affinity-seq data (group #2 in Figure 1D), the CpN is located on the right side of the plus-oriented CTCF consensus motif or the left side of the minus-oriented motif, positioning the CTCF consensus at the entry side of the CpN (Figure 4E, mutCH12, arrow).

Ectopic expression of full-length CTCF (FL-CTCF) in mutCH12 cells restored the open chromatin state and the positioning of several nucleosomes on each side of the 5K lost CTCF sites (Figure 4C, E), further corroborating that both chromatin states depend on CTCF occupancy. When examining nucleosome positioning in mutCH12 cells expressing either a C-terminal truncation (deltaC) or an N-terminal truncation (deltaN) of CTCF, we found that the truncation of the N-terminus prevented the restoration of open chromatin and proper nucleosome positioning around CTCF binding sites. The deltaC truncation also affected nucleosome positioning but to a lesser extent compared to the N-terminus. BORIS, like the N-terminus truncation of CTCF, failed to open chromatin or create phased nucleosome arrays (Figure 4E). Therefore, the MNase-H3-ChIP-seq analysis corroborates our ATAC-seq data, demonstrating that the N-terminus of CTCF is essential for maintaining an open chromatin state and phased nucleosome positioning.

The N-terminus of CTCF is necessary for the recruitment of the chromatin remodeling factor SMARCA5 (Snf2h) at CTCF binding sites

If we assume that CTCF competes with the CpN for DNA binding, the question arises: how does CTCF move the CpN downstream to create open chromatin around its binding site? Previous studies have shown that the chromatin remodeling factor SMARCA5 (Snf2h) is required for CTCF occupancy and for maintaining nucleosome spacing (26,41,42). To investigate how SMARCA5 degradation, using the small molecule proteolysis targeting chimera (PROTAC) system, affects CTCF binding in relation to CTCF interaction with the CpN, we analyzed data from Bomber et.al., (26), applying the same approach as in Figures 3 and 4. CUT&RUN mapping of CTCF binding sites in Kasumi1 cells revealed that CTCF occupancy decreased dramatically—but not entirely—following SMARCA5 depletion (Figure 5A and Supplementary Figure S9A). Interestingly, despite

low CTCF occupancy persisting at most CTCF sites, SMARCA5 degradation led to a significant reduction in both nucleosome positioning and chromatin accessibility (Figure 5A,B and Supplementary Figure S9).

In relation to the CpN, the CTCF-bound consensuses were nucleosome-free before SMARCA5 degradation but remained at the entry side of the nucleosome after SMARCA5 degradation, thus weakening CTCF binding (Figure 5A and Supplementary Figure S9A). This observation aligns well with our data at the 5K lost CTCF sites in mutCH12 cells (Figure 3,4). We hypothesize that with SMARCA5 degradation, CTCF is no longer able to recruit SMARCA5 to displace the CpN and create open chromatin. However, CTCF can still recognize and bind its target sites, which results in a relatively lower occupancy of CTCF binding. This hypothesis is supported by our data showing that the CTCF variant with the truncated N-terminus can still bind the 5K lost CTCF sites in mutCH12 cells (Figure 3E), albeit with lower occupancy compared to full-length CTCF (Supplementary Figure S8A) but is unable to reposition the CpN for strong binding (Figure 4E).

To test our hypothesis and additionally analyze how SMARCA5 occupancy corelates with CTCF occupancy, we performed ChIP-seq with SMARCA5 Abs in both wtCH12 and mutCH12 cells. We found that SMARCA5 occupancy follows CTCF occupancy in all types of CH12 cells at the remaining CTCF binding sites (Figure 5C, top panel). With the loss of CTCF binding at the 5K sites, SMARCA5 occupancy is lost, suggesting that SMARCA5 is recruited by CTCF to chromatin (Figure 5C, lower panel). The ectopic expression of FL-CTCF in mutCH12 cells, restores SMARCA5 occupancy at the 5K lost CTCF sites (Figure 5C, lower panel). However, the truncation of the N-terminus of CTCF or ectopic expression of BORIS in mutCH12 cells failed to restore SMARCA5 occupancy at the 5K CTCF sites (Figure 5C, red arrows). At the same time, the truncation of the C-terminus affected SMARCA5 enrichment, but at lesser extent, probably, because it is affected CTCF binding overall (Figure 5C and Supplementary Figure S8A). As an additional control, we analyzed SMARCA5 occupancy at 199 CTCF binding sites that were irreversibly lost and not restored by ectopic FL-CTCF expression in mutCH12 cells (Supplementary Figure S9D). At these sites, SMARCA5 occupancy was completely absent and not restored, mirroring the pattern observed with the ectopically expressed deltaN CTCF and BORIS. These data suggest that the N-terminus of CTCF is essential for recruiting SMARCA5, which is necessary for opening chromatin and phasing nucleosomes around CTCF binding sites.

The nucleosome-free accessible chromatin facilitates the halting of cohesin extrusion at CTCF binding sites

The N-terminus of CTCF is crucial for halting cohesin-mediated chromatin extrusion, a process essential for mediating 3D genome organization (45,63-65). Moreover, as demonstrated in this study, the N-terminus of CTCF is also required for nucleosome repositioning and the establishment of open chromatin around CTCF binding sites (Figure 3,4). This observation raises an important question: are these two events—chromatin accessibility and cohesin retention at CTCF sites—interconnected?

Recent studies have shown that chromatin accessibility, or open chromatin, is crucial for cohesin retention at CTCF binding sites (66,67). Thus, the retention of cohesin at CTCF sites depends not only on the direct interaction between the SA2–SCC1 subunits and the N-terminus of CTCF, as proposed in Li et.al., (63), but also on the chromatin state of CTCF bound sites.

To evaluate this hypothesis, we examined CTCF binding sites that are unable to retain cohesin. In each cell type, there is a subset of CTCF sites, referred to as CTCF sites depleted of cohesin (CTCFnotRAD21), which neither exhibit cohesin enrichment nor participate in 3D genome organization (45). Genome browser analysis of these CTCFnotRAD21 sites, combined with ATAC-seq data, revealed that they are generally located in regions inaccessible to Tn5-transposase (Figure 5D). Motif analysis of CTCFnotRAD21sites revealed the same core CTCF consensus sequence as found in CTCF sites occupied by cohesin (CTCF/RAD21) (Figure 5E), suggesting that the DNA sequence alone is not sufficient to explain why some CTCF sites are excluded from cohesin occupancy. To extend this analysis on a genome-wide scale, we selected 1,000 CTCF-bound sites with and without cohesin occupancy in wtCH12 cells (Figure 5F). These two groups of CTCF sites were analyzed for nucleosome positioning (MNase-H3) and chromatin accessibility (ATAC-seq), confirming the initial observation that low or absent cohesin occupancy correlates with closed chromatin around CTCF sites (Figure 5F-G). Interestingly, SMARCA5 occupancy was equally present at both groups of CTCF sites (Figure 5G). The same analysis, conducted on two additional cell lines, mES and NIH3T3, yielded similar conclusions: CTCF sites lacking cohesin are linked to reduced chromatin accessibility. (Supplementary Figure S10).

Moreover, in our recent publication, we showed that the ectopic expression of BORIS in NIH3T3 cells increased CTCF occupancy and chromatin accessibility around CTCF sites via the SRCAP-

H2A.Z pathway (23). Cohesin occupancy analysis at these sites revealed that some CTCF sites, depleted of cohesin in NIH3T3 cells (before BORIS expression) converted into CTCF cohesin enriched sites with BORIS expression (NIH3T3+BORIS cells). This conversion was accompanied by chromatin opening around CTCF sites (Supplementary Figure S11A). Conversely, some CTCF/RAD21 sites were converted into CTCFnotRAD21 sites in NIH3T3+BORIS cells compared to NIH3T3+EV cells, a process accompanied by a loss of chromatin accessibility at these CTCF sites (Supplementary Figure S11B).

Thus, nucleosome repositioning and chromatin opening at CTCF binding sites appear to be integral to the halting of cohesin extrusion during 3D genome organization.

CTCF occupancy is largely determined by the permissive epigenetic status around its binding sites

To investigate what preconditions the 5K lost CTCF sites in mutCH12 cells for future CTCF occupancy, we analyzed the CpG methylation status using 5mC MeDIP-seq in both wtCH12 and mutCH12 cells. First, we compared CpG methylation enrichment at CTCF motifs that were either bound or not bound by CTCF in wtCH12 cells (Figure 6A). This analysis revealed a stark difference: CTCF-bound sites were completely depleted of CpG methylation, whereas not bound CTCF sites were highly enriched with CpG methylation. This finding aligns with the well-established fact that CpG methylation negatively affects CTCF binding (21,22). Next, we examined the CpG methylation status across three distinct groups of CTCF binding sites in CH12 cells: (#1) Remaining CTCF sites: 56,276 sites that are bound by CTCF in both wtCH12 and mutCH12 cells; (#2) 5K lost CTCF sites: 4,958 sites that lost CTCF binding in mutCH12 cells but could be restored with ectopic expression of FL-CTCF; (#3) Irreversibly lost CTCF sites: 199 sites that were irreversibly lost in mutCH12 cells and could not be restored with FL-CTCF expression (Figure 6B). The MeDIP-seq analysis demonstrated that while the remaining CTCF sites (#1) were completely devoid of CpG methylation, the 5K lost CTCF sites (#2) began to acquire some CpG methylation in the absence of CTCF, as indicated by the enrichment of MeDIP-seq reads at the CTCF motifs in mutCH12 cells compared to wtCH12 cells (Figure 6B and Supplementary Figure S12A, shown by the black arrow). In contrast, the irreversibly lost CTCF sites (#3) exhibited a more pronounced gain of CpG methylation, which explains why CTCF can no longer bind to these sites (Figure 6B, red arrow).

Previous studies have indicated that the presence of CTCF at unmethylated sites is essential for maintaining their unmethylated state (59,68). However, this raises the question of why only a small subset (199) of the lost 5K CTCF sites gained CpG methylation, while the remaining 4,958 sites remained largely methylation-free. To address this, we first analyzed the sequences of the two groups (#2 and #3) of CTCF sites to determine whether the irreversibly lost CTCF sites might have a higher presence of CpG sites within the consensus sequence, as previously reported (29). No significant differences were observed between these two groups that could explain their differential methylation status (Figure 6C). Furthermore, the irreversibly lost CTCF sites were not associated with CpG islands, with only 3.2% of them being part of such regions. A manual analysis of the most representative examples of irreversibly lost CTCF sites revealed that these 199 sites already exhibited some level of CpG methylation in wtCH12 cells, particularly in the sequences surrounding the CTCF-bound sites (Figure 6B, D and Supplementary Figure S12B, shown by black arrows). This contrasts sharply with the 5K lost sites, which could be restored with FL-CTCF expression and were generally devoid of CpG methylation in both wtCH12 and mutCH12 cells (Figure 6B, D).

Thus, certain CTCF sites are more susceptible to acquiring CpG methylation upon the loss of CTCF binding. Based on the observed CpG methylation enrichment (Figure 6B,D and Supplementary Figure S12B), these sites may initially be hemi-methylated (with only one strand of the DNA being methylated, as shown in Supplementary Figure S12B). Over time, with the loss of CTCF binding, these sites are more likely to become fully CpG methylated, which renders them inaccessible to CTCF binding.

As we have shown that the repressive status of CpN inhibits CTCF binding (Figure 1D and Supplementary Figure S5), we analyzed H3K9me3 in wtCH12 and mutCH12 cells. A comparison of H3K9me3 levels at the remaining and lost CTCF sites in these cells showed that the chromatin status did not change with the deletion of ZFs9-11, nor with the loss of CTCF occupancy at the 5K sites (Figure 6E,F and Supplementary Figure S12C,D). This finding explains why these 5K lost CTCF sites remain available for future CTCF occupancy in mutCH12 cells. However, the 199 irreversibly lost CTCF sites did acquire the repressive histone mark, rendering these sites inaccessible for CTCF occupancy (Figure 6G).

Thus, in this study, we confirmed our initial hypothesis regarding the regulation of CTCF occupancy by CpN. We demonstrated that CTCF binding to the 5K lost CTCF sites in mutCH12 cells is preprogrammed not only by the CpG methylation status of the CTCF site itself but also by the CpG methylation status and histone modifications of the CpN. The preservation of the unchanged CpG methylation status and H3K9me3 histone modifications at the 5K lost CTCF sites in mutCH12 cells makes these sites available for CTCF occupancy (Figure 6). This finding highlights the importance of the epigenetic landscape in regulating CTCF binding and further emphasizes the role of chromatin accessibility in CTCF function.

Discussion

CTCF binding patterns are closely linked to cell fate during differentiation, playing a critical role in 3D genome organization and cell-specific gene transcription (59,69). In this study, we sought to investigate how these cell-specific CTCF binding patterns are established and maintained to preserve cell identity. First, we compared CTCF binding to naked DNA versus chromatin and proposed a model for CTCF occupancy. According to this model, CTCF binding sites are strategically positioned at the entry side of a well-positioned nucleosome, such that upon CTCF binding, its N-terminus is oriented towards the nucleosome. We refer to this nucleosome as the CTCF-priming nucleosome (CpN). CTCF can either shift this nucleosome downstream from its binding site or not, depending on the epigenetic state of the nucleosome.

CTCF displaces the nucleosome when the nucleosomal DNA is free of CpG methylation and the nucleosome lacks repressive histone marks, such as H3K9me3. In this scenario, CTCF recruits SMARCA5 via its N-terminus, pushing the nucleosome downstream and allowing stable binding to the now nucleosome-free sequence. However, CTCF is unable to displace the nucleosome if the nucleosomal DNA is CpG-methylated and enriched with repressive histone marks like H3K9me3. In such cases, the nucleosome remains in place, resulting in weak and transient CTCF binding.

To confirm our model, we used wtCH12 and mutCH12 cells and demonstrated that as long as the CpN's epigenetic status remains favorable for CTCF binding, these sites remain pre-marked for CTCF occupancy, even in the absence of CTCF itself. Our data suggest that both the CTCF

consensus sequence and the CpN must be free of repressive epigenetic marks to permit stable CTCF binding.

We also speculate that the mechanism by which priming nucleosomes regulate CTCF occupancy may extend to other pioneer factors capable of displacing nucleosomes. However, the exact mechanism of nucleosome displacement likely varies, depending on the specific protein partners of each factor. Pioneer factors such as REST (70), PU.1 (71), and ESRRB (72) have been associated with well-positioned nucleosomes. In our study, we demonstrated that the orientation of binding motifs is critical for mapping the priming nucleosome that regulates CTCF binding. However, in the aforementioned studies, the significance of motif orientation has often been overlooked, which may obscure the role of well-positioned nucleosomes flanking one side of the binding motifs when they are not occupied by the factor.

Do small CTCF peaks matter? Cross-referencing ChIP-seq (*in vivo*) with Affinity-seq (*in vitro*) from the same cell type revealed that CTCF sites detected strongly *in vitro* but not *in vivo* are still transiently bound by CTCF *in vivo*. However, this transient CTCF occupancy is often insufficient for these sites to be classified as significantly bound by standard peak-calling algorithms, such as MACS. Similarly, when comparing CTCF occupancy across different cell lines, a closer examination of cell-specific CTCF binding sites shows that these sites are also transiently bound by CTCF in other cell types but are not identified as significant peaks in ChIP-seq data.

In Figure 1D and Supplementary Figures S1-S7, we have highlighted these low-occupancy CTCF sites with yellow arrows. According to our model, CTCF can transiently recognize and bind to these sites without inducing chromatin opening. The repressive nature of the CpN, which incorporates the H3K9me3 repressive histone mark, prevents strong and sustained CTCF occupancy. Thus, we propose that there are many more CTCF binding sites than are currently detected by ChIP-seq using peak-calling algorithms like MACS.

Do these low-occupancy CTCF sites matter? Our data suggest they do. We observed that low CTCF occupancy is associated with low cohesin enrichment, indicating that these sites might contribute to loop formation, albeit transiently and for short durations. A growing body of research supports the idea that low-occupancy CTCF sites play a role in cell-specific transcription (73), serve as targets for JPX RNA (74). Additionally, recent findings indicate that weak CTCF sites help define H3K9me2/3 nanodomain structures within the genome (75). In summary, these low-

occupancy CTCF sites should not be disregarded, as they may contribute to 3D genome organization and gene transcription.

Why does the enrichment of H3K9me3 at the CpN affect CTCF occupancy? In this study, we demonstrated that the presence of the H3K9me3 histone modification on the CTCF priming nucleosome (CpN) either reduces or completely inhibits CTCF binding to chromatin. This finding is consistent with several previous studies that have identified a mutually exclusive relationship between H3K9me3 enrichment and CTCF occupancy (27,75-77). For example, during the differentiation of human embryonic stem cells into pancreatic islet organoids, CTCF recruitment to new binding sites is facilitated by the demethylation of H3K9me3 to H3K9me2 on nucleosomes flanking these sites (76). The H3K9me3 modification can be established by at least six enzymes, including SUV39H1, SUV39H2, SETDB1, SETDB2, G9A, and GLP, which exhibit redundant functions (78). The single knockout of several of these enzymes has been shown to increase CTCF occupancy. For instance, SETDB1 depletion in mouse cells led to the increased recruitment of CTCF at more than 1,600 CTCF motifs within SINE B2 repeats (79). Similar results confirmed that SETDB1 knockout caused a global increase in CTCF occupancy, accompanied by changes in nucleosome positioning around newly occupied CTCF sites, independent of DNA methylation (27). Furthermore, G9A knockout also resulted in enhanced CTCF occupancy (80).

Thus, the removal of H3K9me3 consistently increases CTCF occupancy at thousands of CTCF binding sites, though not universally. This pattern mirrors that observed with CpG methylation, which influences CTCF occupancy but is not sufficient to explain its genome-wide distribution (81). We speculate that the CpN may harbor additional repressive histone marks not mapped in this study.

The reduced CTCF occupancy at sites flanked by H3K9me3-modified nucleosomes suggests that CTCF may bind these sites transiently but is unable to reposition the CpN. As previously shown (26,41), and confirmed by our study, SMARCA5 (SNF2H) is required for CTCF to displace nucleosomes at its binding sites. Interestingly, histone deacetylation has been shown to block SWI/SNF remodelers from accessing chromatin (82), suggesting that repressive histone modifications may hinder SMARCA5-mediated nucleosome displacement, thereby preventing the strong and stable occupancy of CTCF.

Why is the CTCF priming nucleosome well-positioned relative to the CTCF consensus? Our proposed model supports the CTCF-nucleosome competition model, which has been explored in prior studies (35,38,39). An analysis of MNase-seq data from experiments where CTCF was depleted using either the auxin-degron system (83) or a conditional mouse model (84), or where CTCF binding was lost during cell differentiation (40), revealed increased nucleosome occupancy directly at CTCF binding sites in the absence of CTCF. In this study, by sorting CTCF motifs into two groups based on their orientation, we found that the CTCF consensus typically resides at the entry side of the well-positioned nucleosome. Thus, our study is the first to demonstrate that the nucleosome is precisely positioned relative to CTCF motif orientation, with the N-terminus of CTCF facing the nucleosome upon binding.

The next question is: Why is the CTCF priming nucleosome well-positioned? The fact that nucleosomes remain well-positioned even in the absence of CTCF suggests that intrinsic DNA properties, such as DNA conformation and bendability, play a key role in nucleosome positioning. Indeed, CTCF binding sequences have been shown to possess properties that enable them to stall RNA polymerase II independently of CTCF binding (85) and help retain cohesin at CTCF-bound sites (45). Notably, even when CTCF's N-terminus, which interacts with cohesin, is directed to alternative target sites, cohesin is not retained at non-CTCF sequences (45,66), indicating that the specific conformation of the CTCF-DNA complex is crucial. Moreover, the CTCF motif sequence itself has been found to exhibit significantly higher DNA bendability compared to the surrounding 200 bp of DNA (86). DNA bendability is a key factor in nucleosome positioning, and sequences with greater flexibility often favor specific rotational settings within nucleosomes (87). Thus, the high flexibility of the DNA at CTCF consensus sites may naturally favor its positioning near the entry side of the nucleosome.

Another potential explanation for the well-positioned nucleosome could be related to non-B DNA motifs, which are found to be highly enriched at CTCF sites (88,89). Non-B DNA structures are known to disrupt nucleosome positioning (90). If CTCF binding sites adopt a non-B DNA structure, this could act as a repellent for nucleosome assembly, further contributing to the shift in nucleosome positioning relative to the CTCF site.

In summary, our study underscores the critical role of the well-positioned nucleosome in establishing and maintaining CTCF binding patterns, which are crucial for cell identity. We

propose that CTCF binding is tightly regulated by the epigenetic state of the priming nucleosome. The next question is: What factors guide and establish these epigenetic marks during cell differentiation?

Data availability

All raw and processed sequencing data used in this study are available through NCBI GEO database (GSE277826).

Supplementary data

Supplementary Figures S1-S12.

Acknowledgments

This study used the Office of Cyber Infrastructure and Computational Biology High Performance Computing cluster at NIAID, and high-performance computational capabilities of the Biowulf Linux cluster at NIH. Author Contributions: M.T., D.N.B., and Y.J. conducted the experiments. E.M.P. and L.R. performed the bioinformatics analyses. M.T. and E.M.P. conceived and designed the project. V.V.L. provided overall supervision and support. E.M.P. wrote the paper with contributions and corrections from M.T., D.N.B., E.P., Y.J., D.L., V.B.T. All authors reviewed the manuscript.

Funding

This work was supported by the Division of Intramural Research/NIAID/NIH (to V.V.L.). V.B.T. acknowledges the support by Cancer Research UK grants EDDPMA-Nov21/100044 and SEBPCTA- 2022/100001, BBSRC grant BB/X511171/1 and Pancreatic Cancer UK.

Conflict of interest statement

No potential conflict of interest was reported by the authors.

References:

1. de Wit, E., Vos, E.S., Holwerda, S.J., Valdes-Quezada, C., Verstegen, M.J., Teunissen, H., Splinter, E., Wijchers, P.J., Krijger, P.H. and de Laat, W. (2015) CTCF Binding Polarity Determines Chromatin Looping. *Mol Cell*, **60**, 676-684.
2. Rao, S.S., Huntley, M.H., Durand, N.C., Stamenova, E.K., Bochkov, I.D., Robinson, J.T., Sanborn, A.L., Machol, I., Omer, A.D., Lander, E.S. *et al.* (2014) A 3D map of the human genome at kilobase resolution reveals principles of chromatin looping. *Cell*, **159**, 1665-1680.
3. Klenova, E.M., Nicolas, R.H., Paterson, H.F., Carne, A.F., Heath, C.M., Goodwin, G.H., Neiman, P.E. and Lobanenkov, V.V. (1993) CTCF, a conserved nuclear factor required for optimal transcriptional activity of the chicken c-myc gene, is an 11-Zn-finger protein differentially expressed in multiple forms. *Mol Cell Biol*, **13**, 7612-7624.
4. Kim, T.H., Abdullaev, Z.K., Smith, A.D., Ching, K.A., Loukinov, D.I., Green, R.D., Zhang, M.Q., Lobanenkov, V.V. and Ren, B. (2007) Analysis of the vertebrate insulator protein CTCF-binding sites in the human genome. *Cell*, **128**, 1231-1245.
5. Chen, H., Tian, Y., Shu, W., Bo, X. and Wang, S. (2012) Comprehensive identification and annotation of cell type-specific and ubiquitous CTCF-binding sites in the human genome. *PLoS One*, **7**, e41374.
6. Ohlsson, R., Lobanenkov, V. and Klenova, E. (2010) Does CTCF mediate between nuclear organization and gene expression? *Bioessays*, **32**, 37-50.
7. Bell, A.C., West, A.G. and Felsenfeld, G. (1999) The protein CTCF is required for the enhancer blocking activity of vertebrate insulators. *Cell*, **98**, 387-396.
8. Kurukuti, S., Tiwari, V.K., Tavoosidana, G., Pugacheva, E., Murrell, A., Zhao, Z., Lobanenkov, V., Reik, W. and Ohlsson, R. (2006) CTCF binding at the H19 imprinting control region mediates maternally inherited higher-order chromatin conformation to restrict enhancer access to Igf2. *Proc Natl Acad Sci U S A*, **103**, 10684-10689.
9. Lang, F., Li, X., Zheng, W., Li, Z., Lu, D., Chen, G., Gong, D., Yang, L., Fu, J., Shi, P. *et al.* (2017) CTCF prevents genomic instability by promoting homologous recombination-directed DNA double-strand break repair. *Proc Natl Acad Sci U S A*, **114**, 10912-10917.
10. Phillips, J.E. and Corces, V.G. (2009) CTCF: master weaver of the genome. *Cell*, **137**, 1194-1211.
11. Filippova, G.N., Thienes, C.P., Penn, B.H., Cho, D.H., Hu, Y.J., Moore, J.M., Klesert, T.R., Lobanenkov, V.V. and Tapscott, S.J. (2001) CTCF-binding sites flank CTG/CAG repeats and form a methylation-sensitive insulator at the DM1 locus. *Nat Genet*, **28**, 335-343.
12. Pugacheva, E.M., Tiwari, V.K., Abdullaev, Z., Vostrov, A.A., Flanagan, P.T., Quitschke, W.W., Loukinov, D.I., Ohlsson, R. and Lobanenkov, V.V. (2005) Familial cases of point mutations in the XIST promoter reveal a correlation between CTCF binding and pre-emptive choices of X chromosome inactivation. *Hum Mol Genet*, **14**, 953-965.
13. Price, E., Fedida, L.M., Pugacheva, E.M., Ji, Y.J., Loukinov, D. and Lobanenkov, V.V. (2023) An updated catalog of CTCF variants associated with neurodevelopmental disorder phenotypes. *Front Mol Neurosci*, **16**, 1185796.
14. Fang, C., Wang, Z., Han, C., Safgren, S.L., Helmin, K.A., Adelman, E.R., Serafin, V., Basso, G., Eagen, K.P., Gaspar-Maia, A. *et al.* (2020) Cancer-specific CTCF binding facilitates oncogenic transcriptional dysregulation. *Genome Biol*, **21**, 247.

15. Chen, W., Zeng, Y.C., Achinger-Kawecka, J., Campbell, E., Jones, A.K., Stewart, A.G., Khoury, A. and Clark, S.J. (2024) Machine learning enables pan-cancer identification of mutational hotspots at persistent CTCF binding sites. *Nucleic Acids Res*, **52**, 8086-8099.
16. Hansen, A.S. (2020) CTCF as a boundary factor for cohesin-mediated loop extrusion: evidence for a multi-step mechanism. *Nucleus*, **11**, 132-148.
17. Liu, Y., Wan, X., Li, H., Chen, Y., Hu, X., Chen, H., Zhu, D., Li, C. and Zhang, Y. (2023) CTCF coordinates cell fate specification via orchestrating regulatory hubs with pioneer transcription factors. *Cell Rep*, **42**, 113259.
18. Dixon, J.R., Jung, I., Selvaraj, S., Shen, Y., Antosiewicz-Bourget, J.E., Lee, A.Y., Ye, Z., Kim, A., Rajagopal, N., Xie, W. *et al.* (2015) Chromatin architecture reorganization during stem cell differentiation. *Nature*, **518**, 331-336.
19. Stefanova, M.E., Ing-Simmons, E., Stefanov, S., Flyamer, I., Dorado Garcia, H., Schopflin, R., Henssen, A.G., Vaquerizas, J.M. and Mundlos, S. (2023) Doxorubicin Changes the Spatial Organization of the Genome around Active Promoters. *Cells*, **12**.
20. Kantidze, O.L., Luzhin, A.V., Nizovtseva, E.V., Safina, A., Valieva, M.E., Golov, A.K., Velichko, A.K., Lyubitelev, A.V., Feofanov, A.V., Gurova, K.V. *et al.* (2019) The anti-cancer drugs curaxins target spatial genome organization. *Nat Commun*, **10**, 1441.
21. Kanduri, C., Pant, V., Loukinov, D., Pugacheva, E., Qi, C.F., Wolffe, A., Ohlsson, R. and Lobanenkov, V.V. (2000) Functional association of CTCF with the insulator upstream of the H19 gene is parent of origin-specific and methylation-sensitive. *Curr Biol*, **10**, 853-856.
22. Monteagudo-Sanchez, A., Noordermeer, D. and Greenberg, M.V.C. (2024) The impact of DNA methylation on CTCF-mediated 3D genome organization. *Nat Struct Mol Biol*, **31**, 404-412.
23. Pugacheva, E.M., Bhatt, D.N., Rivero-Hinojosa, S., Tajmul, M., Fedida, L., Price, E., Ji, Y., Loukinov, D., Strunnikov, A.V., Ren, B. *et al.* (2024) BORIS/CTCFL epigenetically reprograms clustered CTCF binding sites into alternative transcriptional start sites. *Genome Biol*, **25**, 40.
24. Dephoure, N., Zhou, C., Villen, J., Beausoleil, S.A., Bakalarski, C.E., Elledge, S.J. and Gygi, S.P. (2008) A quantitative atlas of mitotic phosphorylation. *Proc Natl Acad Sci U S A*, **105**, 10762-10767.
25. Ramirez-Cuellar, J., Ferrari, R., Sanz, R.T., Valverde-Santiago, M., Garcia-Garcia, J., Nacht, A.S., Castillo, D., Le Dily, F., Neguembor, M.V., Malatesta, M. *et al.* (2024) LATS1 controls CTCF chromatin occupancy and hormonal response of 3D-grown breast cancer cells. *EMBO J*, **43**, 1770-1798.
26. Bomber, M.L., Wang, J., Liu, Q., Barnett, K.R., Layden, H.M., Hodges, E., Stengel, K.R. and Hiebert, S.W. (2023) Human SMARCA5 is continuously required to maintain nucleosome spacing. *Mol Cell*, **83**, 507-522 e506.
27. Tam, P.L.F., Cheung, M.F., Chan, L.Y. and Leung, D. (2024) Cell-type differential targeting of SETDB1 prevents aberrant CTCF binding, chromatin looping, and cis-regulatory interactions. *Nat Commun*, **15**, 15.
28. Weth, O. and Renkawitz, R. (2011) CTCF function is modulated by neighboring DNA binding factors. *Biochem Cell Biol*, **89**, 459-468.
29. Hashimoto, H., Wang, D., Horton, J.R., Zhang, X., Corces, V.G. and Cheng, X. (2017) Structural Basis for the Versatile and Methylation-Dependent Binding of CTCF to DNA. *Mol Cell*, **66**, 711-720 e713.
30. Filippova, G.N., Fagerlie, S., Klenova, E.M., Myers, C., Dehner, Y., Goodwin, G., Neiman, P.E., Collins, S.J. and Lobanenkov, V.V. (1996) An exceptionally conserved transcriptional repressor, CTCF, employs different combinations of zinc fingers to bind diverged promoter sequences of avian and mammalian c-myc oncogenes. *Mol Cell Biol*, **16**, 2802-2813.
31. Nakahashi, H., Kieffer Kwon, K.R., Resch, W., Vian, L., Dose, M., Stavreva, D., Hakim, O., Pruett, N., Nelson, S., Yamane, A. *et al.* (2013) A genome-wide map of CTCF multivalency redefines the CTCF code. *Cell Rep*, **3**, 1678-1689.

32. Fu, Y., Sinha, M., Peterson, C.L. and Weng, Z. (2008) The insulator binding protein CTCF positions 20 nucleosomes around its binding sites across the human genome. *PLoS Genet*, **4**, e1000138.
33. Stergachis, A.B., Debo, B.M., Haugen, E., Churchman, L.S. and Stamatoyannopoulos, J.A. (2020) Single-molecule regulatory architectures captured by chromatin fiber sequencing. *Science*, **368**, 1449-1454.
34. Lai, B., Gao, W., Cui, K., Xie, W., Tang, Q., Jin, W., Hu, G., Ni, B. and Zhao, K. (2018) Principles of nucleosome organization revealed by single-cell micrococcal nuclease sequencing. *Nature*, **562**, 281-285.
35. Sonmezer, C., Kleinendorst, R., Imanci, D., Barzaghi, G., Villacorta, L., Schubeler, D., Benes, V., Molina, N. and Krebs, A.R. (2021) Molecular Co-occupancy Identifies Transcription Factor Binding Cooperativity In Vivo. *Mol Cell*, **81**, 255-267 e256.
36. Hansen, A.S., Pustova, I., Cattoglio, C., Tjian, R. and Darzacq, X. (2017) CTCF and cohesin regulate chromatin loop stability with distinct dynamics. *Elife*, **6**.
37. Soochit, W., Sleutels, F., Stik, G., Bartkuhn, M., Basu, S., Hernandez, S.C., Merzouk, S., Vidal, E., Boers, R., Boers, J. *et al.* (2021) CTCF chromatin residence time controls three-dimensional genome organization, gene expression and DNA methylation in pluripotent cells. *Nat Cell Biol*, **23**, 881-893.
38. Voong, L.N., Xi, L., Sebeson, A.C., Xiong, B., Wang, J.P. and Wang, X. (2016) Insights into Nucleosome Organization in Mouse Embryonic Stem Cells through Chemical Mapping. *Cell*, **167**, 1555-1570 e1515.
39. Wiehle, L., Thorn, G.J., Raddatz, G., Clarkson, C.T., Rippe, K., Lyko, F., Breiling, A. and Teif, V.B. (2019) DNA (de)methylation in embryonic stem cells controls CTCF-dependent chromatin boundaries. *Genome Res*, **29**, 750-761.
40. Clarkson, C.T., Deeks, E.A., Samarista, R., Mamayusupova, H., Zhurkin, V.B. and Teif, V.B. (2019) CTCF-dependent chromatin boundaries formed by asymmetric nucleosome arrays with decreased linker length. *Nucleic Acids Res*, **47**, 11181-11196.
41. Wiechens, N., Singh, V., Gkikopoulos, T., Schofield, P., Rocha, S. and Owen-Hughes, T. (2016) The Chromatin Remodelling Enzymes SNF2H and SNF2L Position Nucleosomes adjacent to CTCF and Other Transcription Factors. *PLoS Genet*, **12**, e1005940.
42. Barisic, D., Stadler, M.B., Iurlaro, M. and Schubeler, D. (2019) Mammalian ISWI and SWI/SNF selectively mediate binding of distinct transcription factors. *Nature*, **569**, 136-140.
43. Oomen, M.E., Hansen, A.S., Liu, Y., Darzacq, X. and Dekker, J. (2019) CTCF sites display cell cycle-dependent dynamics in factor binding and nucleosome positioning. *Genome Res*, **29**, 236-249.
44. Nora, E.P., Goloborodko, A., Valton, A.L., Gibcus, J.H., Uebersohn, A., Abdennur, N., Dekker, J., Mirny, L.A. and Bruneau, B.G. (2017) Targeted Degradation of CTCF Decouples Local Insulation of Chromosome Domains from Genomic Compartmentalization. *Cell*, **169**, 930-944 e922.
45. Pugacheva, E.M., Kubo, N., Loukinov, D., Tajmul, M., Kang, S., Kovalchuk, A.L., Strunnikov, A.V., Zentner, G.E., Ren, B. and Lobanenkov, V.V. (2020) CTCF mediates chromatin looping via N-terminal domain-dependent cohesin retention. *Proc Natl Acad Sci U S A*, **117**, 2020-2031.
46. Vian, L., Pekowska, A., Rao, S.S.P., Kieffer-Kwon, K.R., Jung, S., Baranello, L., Huang, S.C., El Khattabi, L., Dose, M., Pruett, N. *et al.* (2018) The Energetics and Physiological Impact of Cohesin Extrusion. *Cell*, **173**, 1165-1178 e1120.
47. Buenrostro, J.D., Giresi, P.G., Zaba, L.C., Chang, H.Y. and Greenleaf, W.J. (2013) Transposition of native chromatin for fast and sensitive epigenomic profiling of open chromatin, DNA-binding proteins and nucleosome position. *Nat Methods*, **10**, 1213-1218.
48. Zuo, Z., Billings, T., Walker, M., Petkov, P.M., Fordyce, P.M. and Stormo, G.D. (2023) On the dependent recognition of some long zinc finger proteins. *Nucleic Acids Res*, **51**, 5364-5376.

49. Shen, Y., Yue, F., McCleary, D.F., Ye, Z., Edsall, L., Kuan, S., Wagner, U., Dixon, J., Lee, L., Lobanenkov, V.V. *et al.* (2012) A map of the cis-regulatory sequences in the mouse genome. *Nature*, **488**, 116-120.
50. Sundaram, V., Cheng, Y., Ma, Z., Li, D., Xing, X., Edge, P., Snyder, M.P. and Wang, T. (2014) Widespread contribution of transposable elements to the innovation of gene regulatory networks. *Genome Res*, **24**, 1963-1976.
51. Fischer, V., Plassard, D., Ye, T., Reina-San-Martin, B., Stierle, M., Tora, L. and Devys, D. (2021) The related coactivator complexes SAGA and ATAC control embryonic stem cell self-renewal through acetyltransferase-independent mechanisms. *Cell Rep*, **36**, 109598.
52. Langmead, B., Trapnell, C., Pop, M. and Salzberg, S.L. (2009) Ultrafast and memory-efficient alignment of short DNA sequences to the human genome. *Genome Biol*, **10**, R25.
53. Li, H., Handsaker, B., Wysoker, A., Fennell, T., Ruan, J., Homer, N., Marth, G., Abecasis, G., Durbin, R. and Genome Project Data Processing, S. (2009) The Sequence Alignment/Map format and SAMtools. *Bioinformatics*, **25**, 2078-2079.
54. Ramirez, F., Dundar, F., Diehl, S., Gruning, B.A. and Manke, T. (2014) deepTools: a flexible platform for exploring deep-sequencing data. *Nucleic Acids Res*, **42**, W187-191.
55. Zhang, Y., Liu, T., Meyer, C.A., Eeckhoute, J., Johnson, D.S., Bernstein, B.E., Nusbaum, C., Myers, R.M., Brown, M., Li, W. *et al.* (2008) Model-based analysis of ChIP-Seq (MACS). *Genome Biol*, **9**, R137.
56. Robinson, J.T., Thorvaldsdottir, H., Winckler, W., Guttman, M., Lander, E.S., Getz, G. and Mesirov, J.P. (2011) Integrative genomics viewer. *Nat Biotechnol*, **29**, 24-26.
57. Quinlan, A.R. and Hall, I.M. (2010) BEDTools: a flexible suite of utilities for comparing genomic features. *Bioinformatics*, **26**, 841-842.
58. Bailey, T.L., Boden, M., Buske, F.A., Frith, M., Grant, C.E., Clementi, L., Ren, J., Li, W.W. and Noble, W.S. (2009) MEME SUITE: tools for motif discovery and searching. *Nucleic Acids Res*, **37**, W202-208.
59. Xiang, J.F. and Corces, V.G. (2021) Regulation of 3D chromatin organization by CTCF. *Curr Opin Genet Dev*, **67**, 33-40.
60. Pugacheva, E.M., Rivero-Hinojosa, S., Espinoza, C.A., Mendez-Catala, C.F., Kang, S., Suzuki, T., Kosaka-Suzuki, N., Robinson, S., Nagarajan, V., Ye, Z. *et al.* (2015) Comparative analyses of CTCF and BORIS occupancies uncover two distinct classes of CTCF binding genomic regions. *Genome Biol*, **16**, 161.
61. Loukinov, D.I., Pugacheva, E., Vatolin, S., Pack, S.D., Moon, H., Chernukhin, I., Mannan, P., Larsson, E., Kanduri, C., Vostrov, A.A. *et al.* (2002) BORIS, a novel male germ-line-specific protein associated with epigenetic reprogramming events, shares the same 11-zinc-finger domain with CTCF, the insulator protein involved in reading imprinting marks in the soma. *Proc Natl Acad Sci U S A*, **99**, 6806-6811.
62. Weth, O., Paprotka, C., Gunther, K., Schulte, A., Baierl, M., Leers, J., Galjart, N. and Renkawitz, R. (2014) CTCF induces histone variant incorporation, erases the H3K27me3 histone mark and opens chromatin. *Nucleic Acids Res*, **42**, 11941-11951.
63. Li, Y., Haarhuis, J.H.I., Sedeno Cacciatore, A., Oldenkamp, R., van Ruiten, M.S., Willems, L., Teunissen, H., Muir, K.W., de Wit, E., Rowland, B.D. *et al.* (2020) The structural basis for cohesin-CTCF-anchored loops. *Nature*, **578**, 472-476.
64. Nora, E.P., Caccianini, L., Fudenberg, G., So, K., Kameswaran, V., Nagle, A., Uebersohn, A., Hajj, B., Saux, A.L., Coulon, A. *et al.* (2020) Molecular basis of CTCF binding polarity in genome folding. *Nat Commun*, **11**, 5612.

65. Nishana, M., Ha, C., Rodriguez-Hernaez, J., Ranjbaran, A., Chio, E., Nora, E.P., Badri, S.B., Kloetgen, A., Bruneau, B.G., Tsirigos, A. *et al.* (2020) Defining the relative and combined contribution of CTCF and CTCFL to genomic regulation. *Genome Biol*, **21**, 108.
66. Do, C., Jiang, G., Cova, G., Katsifis, C.C., Narducci, D.N., Yang, J., Sakellaropoulos, T., Vidal, R., Lhoumaud, P., Tsirigos, A. *et al.* (2024) Brain and cancer associated binding domain mutations provide insight into CTCF's relationship with chromatin and its ability to act as a chromatin organizer. *Res Sq*.
67. Iurlaro, M., Masoni, F., Flyamer, I.M., Wirbelauer, C., Iskar, M., Burger, L., Giorgetti, L. and Schubeler, D. (2024) Systematic assessment of ISWI subunits shows that NURF creates local accessibility for CTCF. *Nat Genet*, **56**, 1203-1212.
68. Kemp, C.J., Moore, J.M., Moser, R., Bernard, B., Teater, M., Smith, L.E., Rabaia, N.A., Gurley, K.E., Guinney, J., Busch, S.E. *et al.* (2014) CTCF haploinsufficiency destabilizes DNA methylation and predisposes to cancer. *Cell Rep*, **7**, 1020-1029.
69. Arzate-Mejia, R.G., Recillas-Targa, F. and Corces, V.G. (2018) Developing in 3D: the role of CTCF in cell differentiation. *Development*, **145**.
70. Harwood, J.C., Kent, N.A., Allen, N.D. and Harwood, A.J. (2019) Nucleosome dynamics of human iPSC during neural differentiation. *EMBO Rep*, **20**.
71. Barozzi, I., Simonatto, M., Bonifacio, S., Yang, L., Rohs, R., Ghisletti, S. and Natoli, G. (2014) Coregulation of transcription factor binding and nucleosome occupancy through DNA features of mammalian enhancers. *Mol Cell*, **54**, 844-857.
72. Festuccia, N., Owens, N., Papadopoulou, T., Gonzalez, I., Tachtsidi, A., Vandoermel-Pournin, S., Gallego, E., Gutierrez, N., Dubois, A., Cohen-Tannoudji, M. *et al.* (2019) Transcription factor activity and nucleosome organization in mitosis. *Genome Res*, **29**, 250-260.
73. Essien, K., Vigneau, S., Apreleva, S., Singh, L.N., Bartolomei, M.S. and Hannenhalli, S. (2009) CTCF binding site classes exhibit distinct evolutionary, genomic, epigenomic and transcriptomic features. *Genome Biol*, **10**, R131.
74. Oh, H.J., Aguilar, R., Kesner, B., Lee, H.G., Kriz, A.J., Chu, H.P. and Lee, J.T. (2021) Jpx RNA regulates CTCF anchor site selection and formation of chromosome loops. *Cell*, **184**, 6157-6173 e6124.
75. Thorn, G.J., Clarkson, C.T., Rademacher, A., Mamayusupova, H., Schotta, G., Rippe, K. and Teif, V.B. (2022) DNA sequence-dependent formation of heterochromatin nanodomains. *Nat Commun*, **13**, 1861.
76. Lyu, X., Rowley, M.J., Kulik, M.J., Dalton, S. and Corces, V.G. (2023) Regulation of CTCF loop formation during pancreatic cell differentiation. *Nat Commun*, **14**, 6314.
77. Jiang, Y., Loh, Y.E., Rajarajan, P., Hirayama, T., Liao, W., Kassim, B.S., Javidfar, B., Hartley, B.J., Kleofas, L., Park, R.B. *et al.* (2017) The methyltransferase SETDB1 regulates a large neuron-specific topological chromatin domain. *Nat Genet*, **49**, 1239-1250.
78. Padeken, J., Methot, S.P. and Gasser, S.M. (2022) Establishment of H3K9-methylated heterochromatin and its functions in tissue differentiation and maintenance. *Nat Rev Mol Cell Biol*, **23**, 623-640.
79. Gualdrini, F., Polletti, S., Simonatto, M., Prosperini, E., Pileri, F. and Natoli, G. (2022) H3K9 trimethylation in active chromatin restricts the usage of functional CTCF sites in SINE B2 repeats. *Genes Dev*, **36**, 414-432.
80. Jiang, Q., Ang, J.Y.J., Lee, A.Y., Cao, Q., Li, K.Y., Yip, K.Y. and Leung, D.C.Y. (2020) G9a Plays Distinct Roles in Maintaining DNA Methylation, Retrotransposon Silencing, and Chromatin Looping. *Cell Rep*, **33**, 108315.
81. Maurano, M.T., Wang, H., John, S., Shafer, A., Canfield, T., Lee, K. and Stamatoyannopoulos, J.A. (2015) Role of DNA Methylation in Modulating Transcription Factor Occupancy. *Cell Rep*, **12**, 1184-1195.

82. Sahu, R.K., Dhakshnamoorthy, J., Jain, S., Folco, H.D., Wheeler, D. and Grewal, S.I.S. (2024) Nucleosome remodeler exclusion by histone deacetylation enforces heterochromatic silencing and epigenetic inheritance. *Mol Cell*.
83. Owens, N., Papadopoulou, T., Festuccia, N., Tachtsidi, A., Gonzalez, I., Dubois, A., Vandormael-Pournin, S., Nora, E.P., Bruneau, B.G., Cohen-Tannoudji, M. *et al.* (2019) CTCF confers local nucleosome resiliency after DNA replication and during mitosis. *Elife*, **8**.
84. Marina-Zarate, E., Rodriguez-Ronchel, A., Gomez, M.J., Sanchez-Cabo, F. and Ramiro, A.R. (2023) Low-affinity CTCF binding drives transcriptional regulation whereas high-affinity binding encompasses architectural functions. *iScience*, **26**, 106106.
85. Luan, J., Xiang, G., Gomez-Garcia, P.A., Tome, J.M., Zhang, Z., Vermunt, M.W., Zhang, H., Huang, A., Keller, C.A., Giardine, B.M. *et al.* (2021) Distinct properties and functions of CTCF revealed by a rapidly inducible degron system. *Cell Rep*, **34**, 108783.
86. Li, K., Carroll, M., Vafabakhsh, R., Wang, X.A. and Wang, J.P. (2022) DNAcycP: a deep learning tool for DNA cyclizability prediction. *Nucleic Acids Res*, **50**, 3142-3154.
87. Biswas, A. and Basu, A. (2023) The impact of the sequence-dependent physical properties of DNA on chromatin dynamics. *Curr Opin Struct Biol*, **83**, 102698.
88. Georgakopoulos-Soares, I., Victorino, J., Parada, G.E., Agarwal, V., Zhao, J., Wong, H.Y., Umar, M.I., Elor, O., Muhwezi, A., An, J.Y. *et al.* (2022) High-throughput characterization of the role of non-B DNA motifs on promoter function. *Cell Genom*, **2**.
89. Hou, Y., Li, F., Zhang, R., Li, S., Liu, H., Qin, Z.S. and Sun, X. (2019) Integrative characterization of G-Quadruplexes in the three-dimensional chromatin structure. *Epigenetics*, **14**, 894-911.
90. Kouzine, F., Wojtowicz, D., Baranello, L., Yamane, A., Nelson, S., Resch, W., Kieffer-Kwon, K.R., Benham, C.J., Casellas, R., Przytycka, T.M. *et al.* (2017) Permanganate/S1 Nuclease Footprinting Reveals Non-B DNA Structures with Regulatory Potential across a Mammalian Genome. *Cell Syst*, **4**, 344-356 e347.

Main Figures

Figure 1

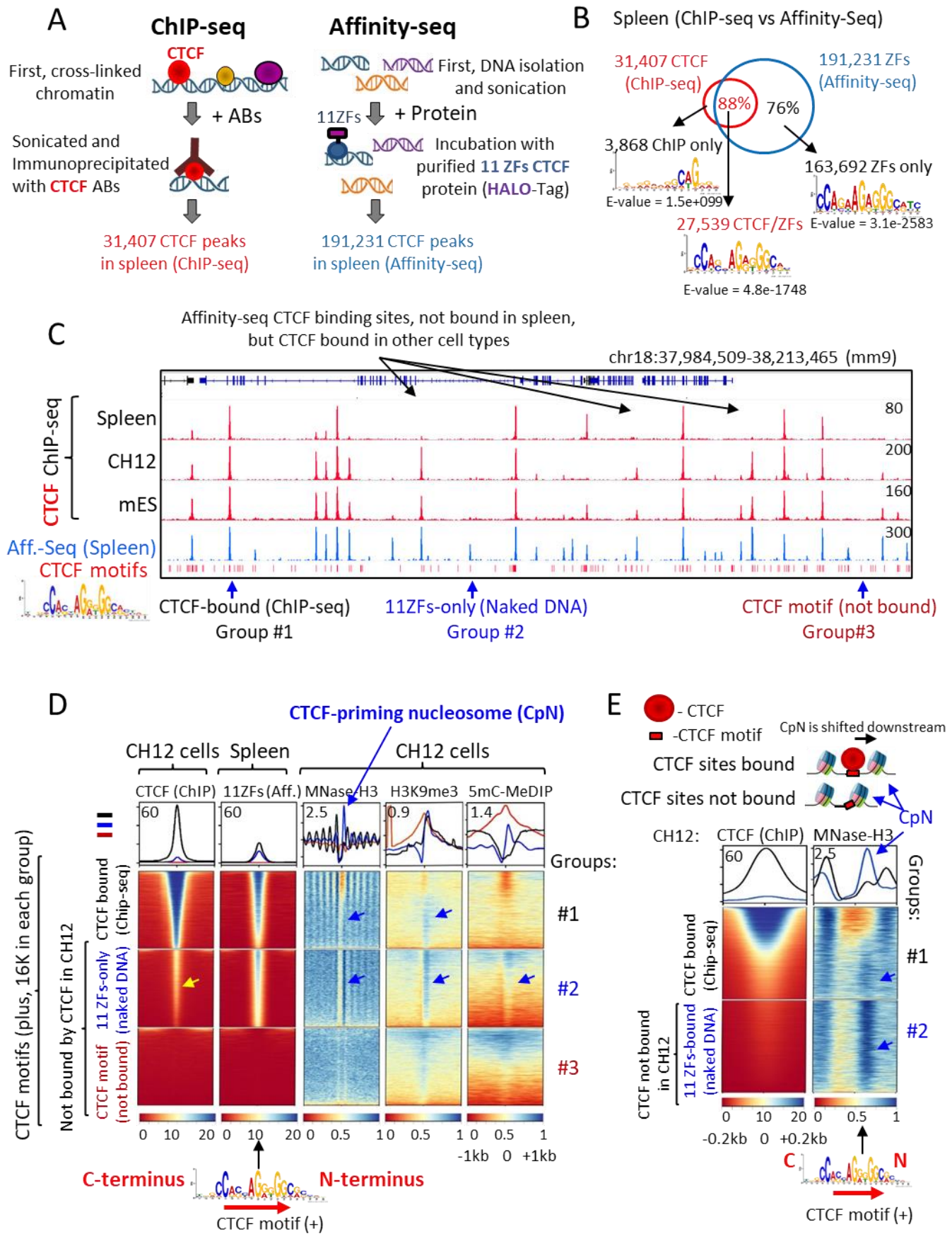
A
ChIP-seq
Affinity-seq
CTCF
First, cross-linked chromatin
+ ABs
Sonicated and Immunoprecipitated with CTCF ABs
31,407 CTCF peaks in spleen (ChIP-seq)
First, DNA isolation and sonication
11ZFs
+ Protein
Incubation with purified 11 ZFs CTCF protein (HALO-Tag)
191,231 CTCF peaks in spleen (Affinity-seq)
B
Spleen (ChIP-seq vs Affinity-Seq)
31,407 CTCF (ChIP-seq)
191,231 ZFs (Affinity-seq)
88%
76%
3,868 ChIP only
E-value = 1.5e+099
163,692 ZFs only
E-value = 3.1e-2583
27,539 CTCF/ZFs
E-value = 4.8e-1748
C
Affinity-seq CTCF binding sites, not bound in spleen, but CTCF bound in other cell types
chr18:37,984,509-38,213,465 (mm9)
CTCF ChIP-seq
Spleen
CH12
mES
Aff.-Seq (Spleen)
CTCF motifs
80
200
160
300
CTCF-bound (ChIP-seq)
Group #1
11ZFs-only (Naked DNA)
Group #2
CTCF motif (not bound)
Group#3
D
CTCF-priming nucleosome (CpN)
CH12 cells
Spleen
CH12 cells
CTCF (ChIP)
11ZFs (Aff.)
MNase-H3
H3K9me3
5mC-MeDIP
60
60
2.5
0.9
1.4
Groups:
#1
#2
#3
CTCF motifs (plus, 16K in each group)
Not bound by CTCF in CH12
CTCF bound (Chip-seq)
11 ZFs-only (naked DNA)
CTCF motif (not bound)
0 10 20 0 10 20 0 0.5 1 0 0.5 1 0 0.5 1
-1kb 0 +1kb
C-terminus
N-terminus
CTCF motif (+)
E
- CTCF
-CTCF motif
CpN is shifted downstream
CTCF sites bound
CTCF sites not bound
CpN
CH12:
CTCF (ChIP)
MNase-H3
60
2.5
Groups:
#1
#2
CTCF bound (Chip-seq)
CTCF not bound in CH12
11 ZFs-bound (naked DNA)
0 10 20 0 0.5 1
-0.2kb 0 +0.2kb
C
N
CTCF motif (+)

Figure 1. CTCF binding sites are strategically positioned at the entry site of well-positioned nucleosome. (A) Schematic comparison of ChIP-seq and Affinity-seq approaches used to map CTCF binding sites in mouse spleen. **(B)** Venn diagram illustrating the overlap between CTCF binding sites identified by ChIP-seq and Affinity-seq. MEME motifs enriched in each group of CTCF sites are indicated by black arrows. **(C)** Representative genome browser view displaying CTCF ChIP-seq data (red) compared to CTCF Affinity-seq data (Aff.-seq, blue). The red bars at the bottom show the 15bp-CTCF motif sequences present in the mouse genome (mm9). Blue arrows highlight examples of CTCF binding sites categorized into three groups, as analyzed in panel **(D). (D)** Heatmaps centered on the CTCF motif in the plus (sense) orientation, showing (from left to right): CTCF ChIP-seq (CH12 cells), CTCF Affinity-seq (spleen), MNase-H3 nucleosome positioning, H3K9me3 ChIP-seq, and 5mC MeDIP-seq data (CH12 cells). These data are aligned across three groups of CTCF binding sites: (#1) CTCF-bound sites in CH12 cells (black), (#2) Affinity-seq recovered CTCF sites that were not identified as peaks by MACS in CTCF ChIP-seq of CH12 cells (blue), and (#3) CTCF motifs neither bound by CTCF nor recovered by Affinity-seq (red). The CTCF priming nucleosome (CpN) is indicated by a blue arrow. The low CTCF ChIP-seq signal at the 11 ZFs-only group (#2) is shown by a yellow arrow. **(E)** A zoomed-in view of data from the panel **(D)**, focusing on a 400 bp window centered on the plus CTCF motif. This panel combines CTCF ChIP-seq data with MNase-H3 data from CH12 cells to illustrate the downstream shift of well-positioned nucleosomes from the CTCF-bound motifs. At CTCF motifs recovered by Affinity-seq but not bound by CTCF in CH12 cells, this nucleosome is positioned at the entry site of the plus CTCF motif, with the N-terminus oriented toward the CpN (indicated by a blue arrow). A schematic representation of bound and unbound CTCF sites is provided at the top.

Figure 2

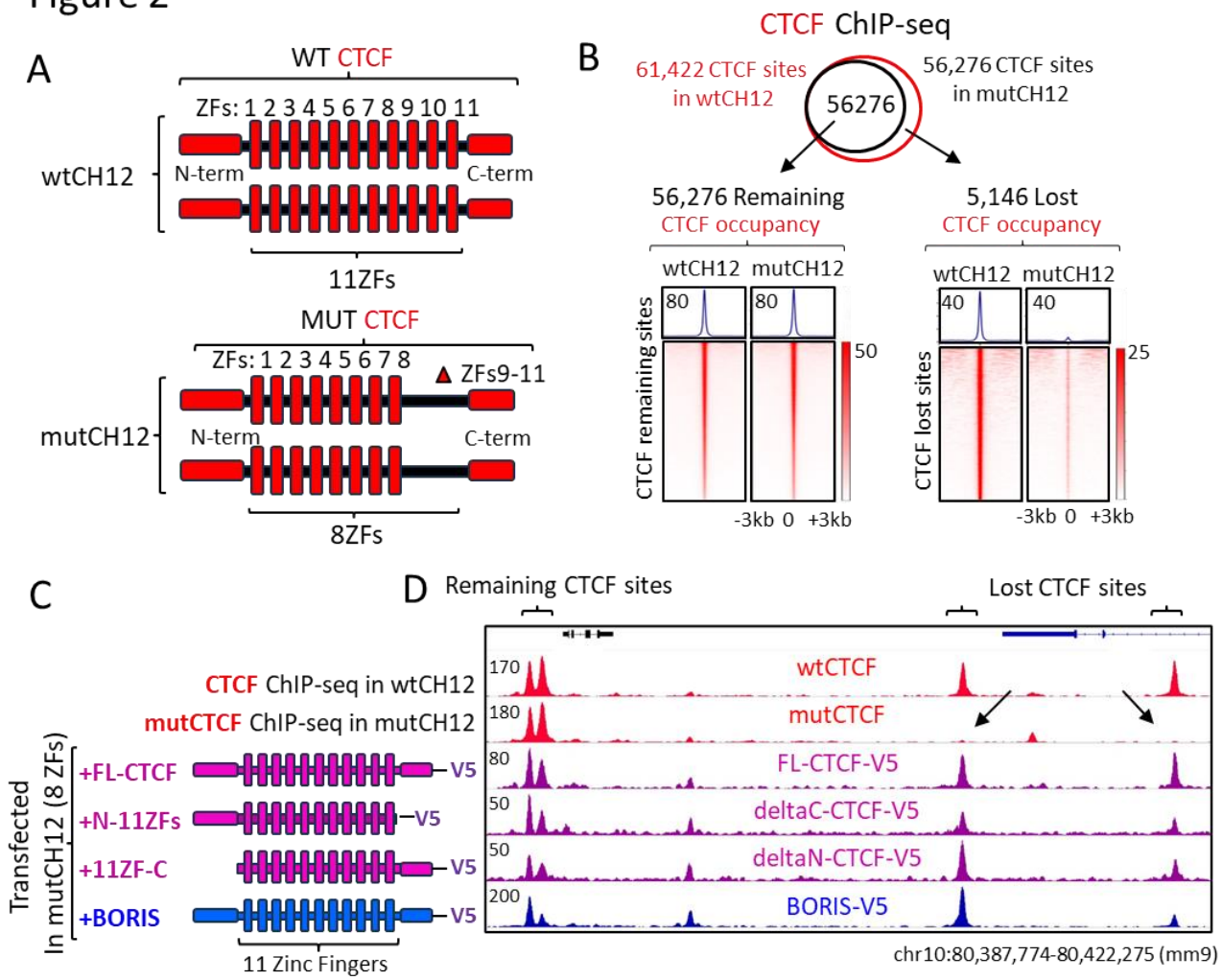

Figure 2. CH12 cell line-based system to study CTCF interaction with chromatin. (A) Schematic representations of wild-type and mutant CTCF proteins in wtCH12 and mutCH12 cells, respectively. The mutant CTCF has a homozygous deletion of zinc fingers 9-11 (ZFs 9-11). **(B)** Top: Venn diagram illustrating the overlap of CTCF binding sites mapped in wtCH12 versus mutCH12 cells. Bottom: Heatmap displaying CTCF occupancy in wtCH12 and mutCH12 cells at sites where CTCF binding is either remained or lost. **(C)** Schematic representation of CTCF variants and BORIS ectopically expressed in mutCH12 cells. All ectopically expressed proteins were tagged with a V5-tag to allow mapping of their binding sites by ChIP-seq independent from endogenous CTCF. **(D)** Genome browser view showing examples of the 5K CTCF binding sites lost in mutCH12 cells, which were restored by ectopic expression of different CTCF variants and BORIS, as depicted in panel (C). The lost CTCF sites in mutCH12 cells are shown by black arrows.

Figure 3

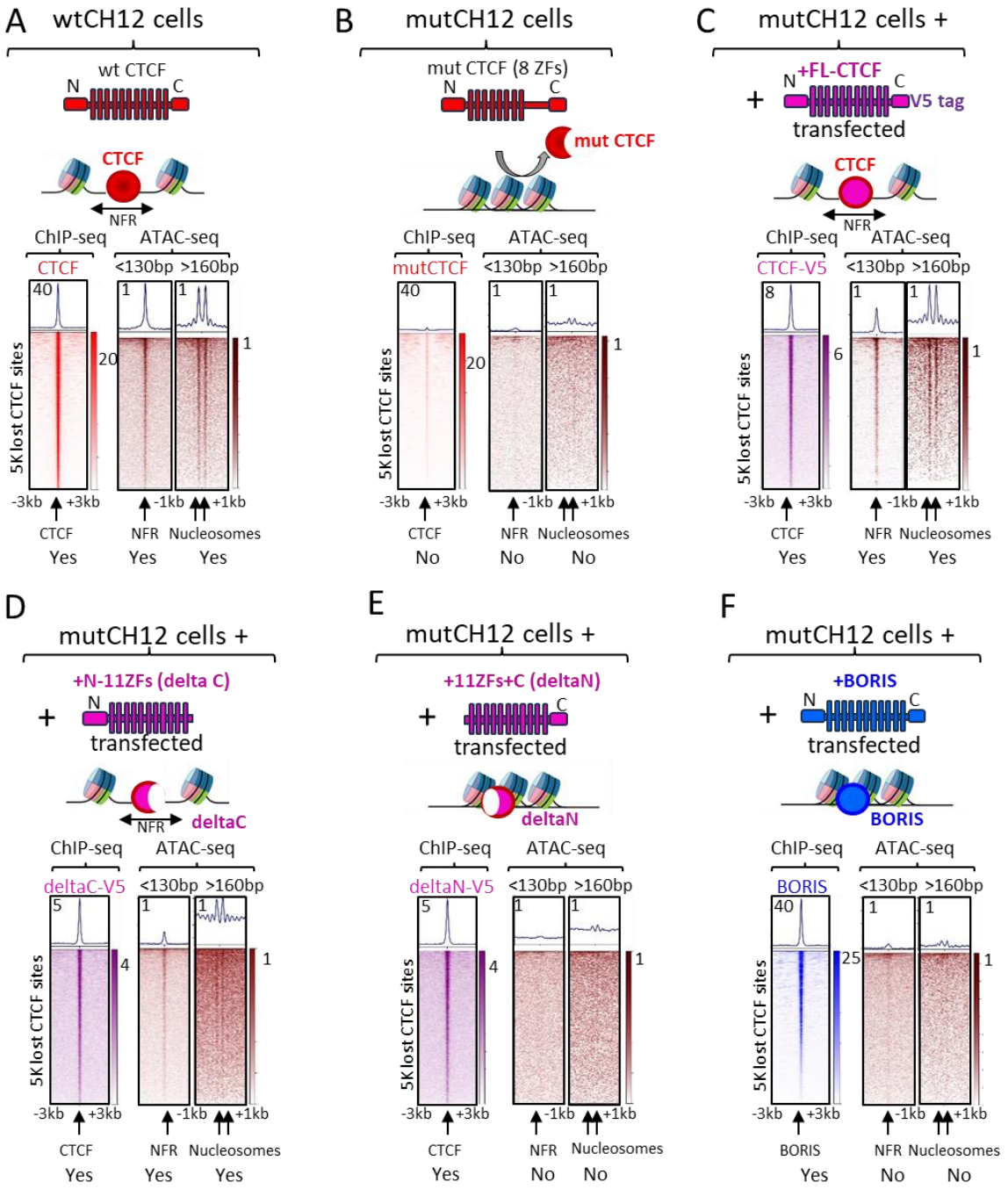

Figure 3. Chromatin accessibility around CTCF binding sites depends on the N-terminus of CTCF. (A-F) Analysis of the 5K lost CTCF sites using ATAC-seq data combined with ChIP-seq data in various conditions: **(A)** wtCH12 cells, **(B)** mutCH12 cells, **(C)** mutCH12 cells ectopically expressing full-length CTCF (FL-CTCF), **(D)** mutCH12 cells ectopically expressing CTCF with a truncated C-terminus (deltaC), **(E)** mutCH12 cells ectopically expressing CTCF with a truncated N-terminus (deltaN), and **(F)** mutCH12 cells ectopically expressing human BORIS. At the top of

each panel, a schematic representation of the protein mapped by ChIP-seq is shown, with its occupancy at the 5K lost sites depicted by a heatmap labeled "ChIP-seq." Below the protein structure, a schematic of the proposed binding of the protein in relation to nucleosome positioning and open chromatin states, as mapped by ATAC-seq, is presented, with the corresponding heatmap shown beneath. Paired-end mapped ATAC-seq reads were divided into short fragments (<130 bp), indicative of CTCF footprint, and nucleosome-sized fragments (>160 bp) to determine nucleosome positioning. The presence of Nucleosome-Free Regions (NFR) and the two flanking nucleosomes around CTCF binding sites is indicated by black arrows, with a "Yes" if present or a "No" if absent. The heatmaps are centered at the summit of the 5K lost CTCF sites. Endogenous CTCF and ectopically expressed CTCF variants are highlighted in red and purple, respectively. BORIS occupancy is highlighted in blue.

Figure 4

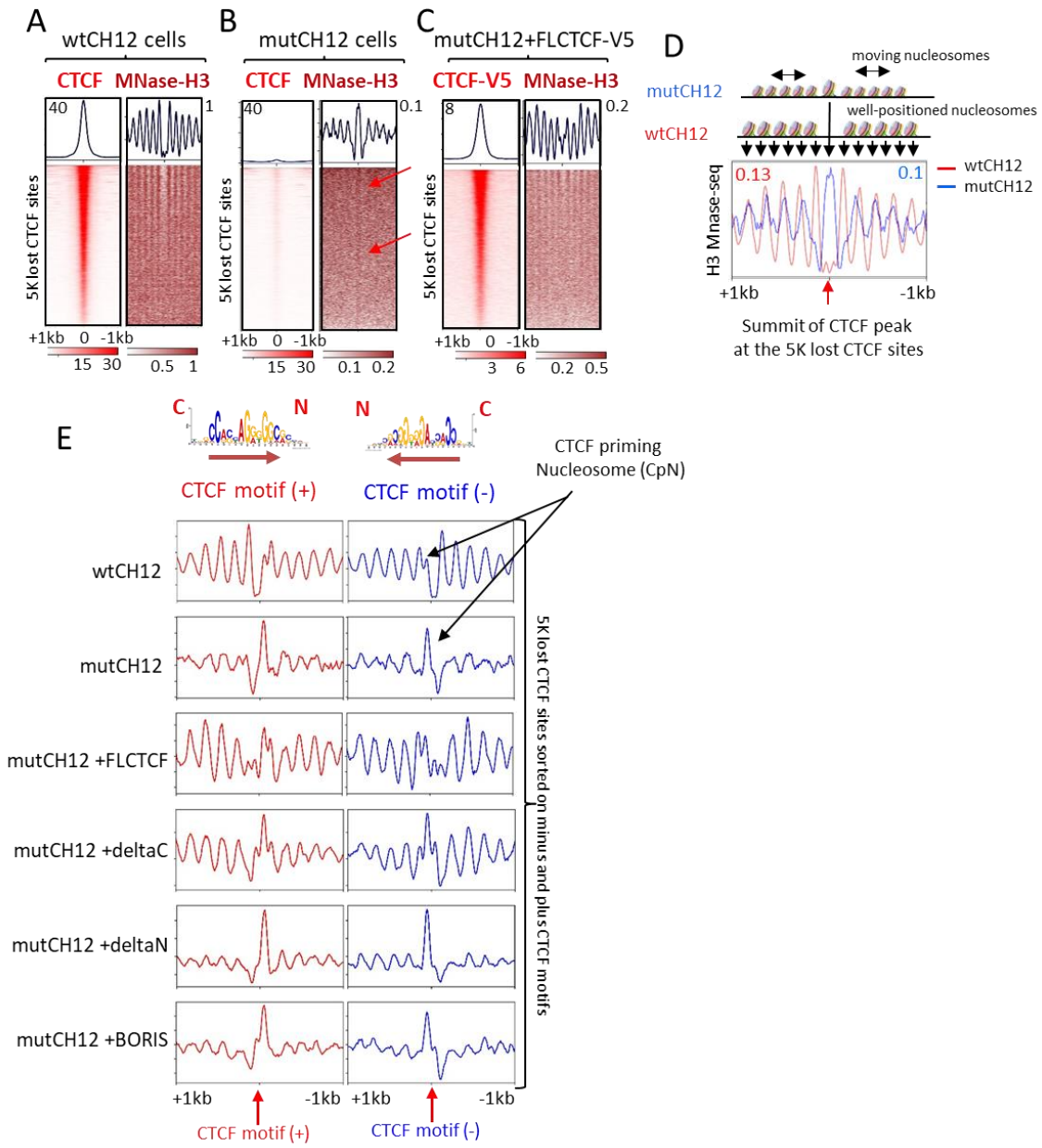

Figure 4. Nucleosome positioning around CTCF binding sites depends on the N-terminus of CTCF. (A-C) Heatmaps displaying CTCF occupancy (ChIP-seq) combined with nucleosome positioning, mapped by MNase-seq assisted H3 histone ChIP sequencing (MNase-H3), at the summit of the 5K lost CTCF sites in wtCH12 **(A)** versus mutCH12 cells **(B)**. In mutCH12 cells ectopically expressing full-length CTCF (FL-CTCF) **(C)**, CTCF occupancy is mapped using V5-tag antibodies. Red arrows indicate the presence of a well-positioned nucleosome directly at CTCF binding sites in mutCH12 cells, which is absent in wtCH12 cells. **(D)** MNase-H3 ChIP-seq profile showing nucleosome occupancy at the lost 5K CTCF sites in wtCH12 cells compared to mutCH12 cells. At the top, a schematic representation of nucleosome positioning at the lost CTCF sites is provided, highlighting a well-positioned nucleosome (larger size nucleosome) directly at the lost CTCF sites in mutCH12 cells. **(E)** MNase-H3 ChIP-seq profile of nucleosome occupancy centered at the lost CTCF motifs, separated into plus and minus orientations (schematic of CTCF motifs shown at the top). The cell types are labeled on the left, and the CTCF priming nucleosome is indicated by black arrows.

Figure 5

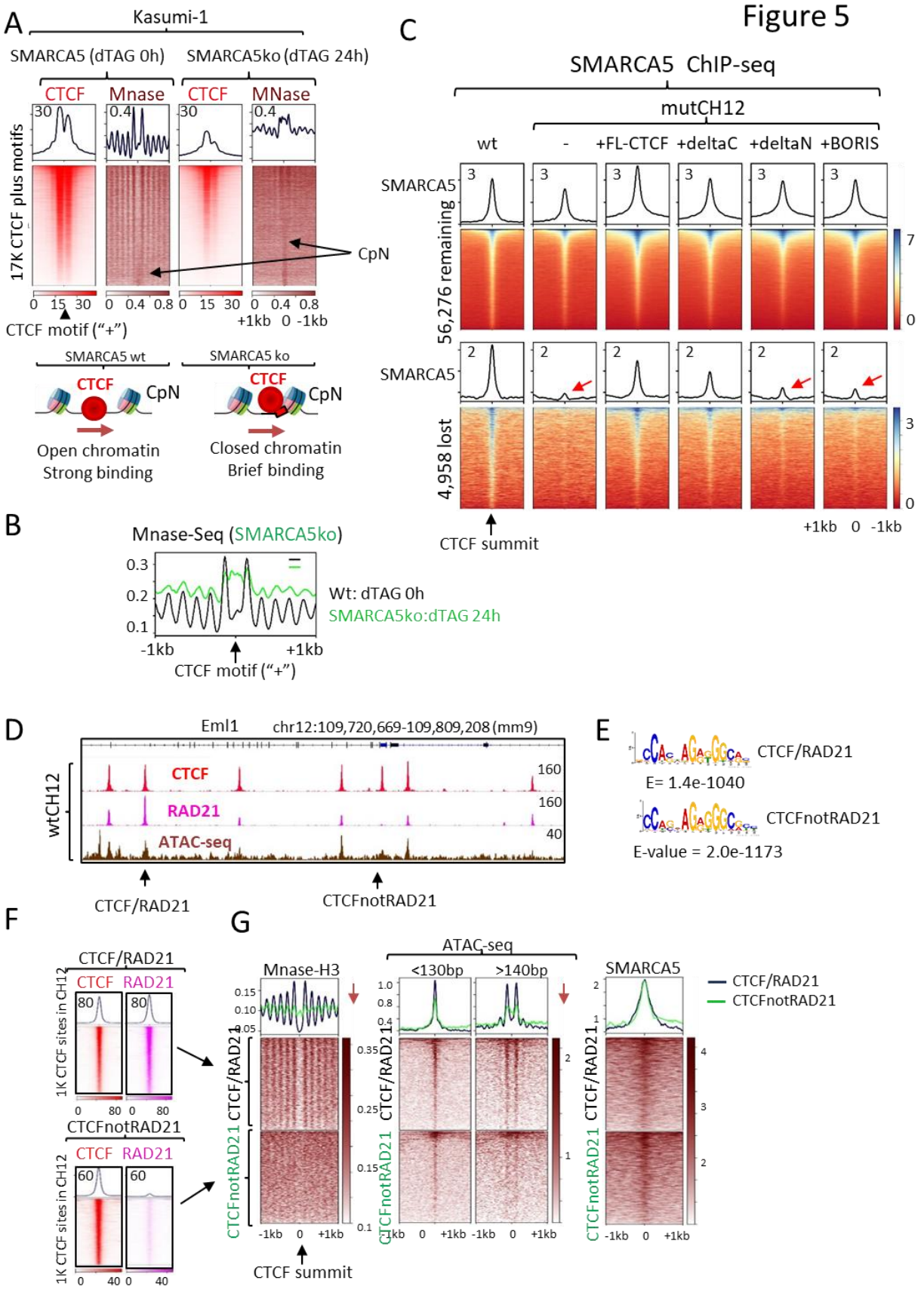
A
Kasumi-1
SMARCA5 (dTAG 0h)
SMARCA5ko (dTAG 24h)
CTCF
Mnase
CTCF
MNase
17K CTCF plus motifs
CpN
CTCF motif ("+")
+1kb 0 -1kb
SMARCA5 wt
SMARCA5 ko
CTCF
CpN
Open chromatin
Strong binding
Closed chromatin
Brief binding
B
Mnase-Seq (SMARCA5ko)
Wt: dTAG 0h
SMARCA5ko:dTAG 24h
-1kb
+1kb
CTCF motif ("+")
C
SMARCA5 ChIP-seq
mutCH12
wt
-
+FL-CTCF
+deltaC
+deltaN
+BORIS
SMARCA5
56,276 remaining
SMARCA5
4,958 lost
CTCF summit
+1kb 0 -1kb
D
Eml1
chr12:109,720,669-109,809,208 (mm9)
wtCH12
CTCF
RAD21
ATAC-seq
CTCF/RAD21
CTCFnotRAD21
E
CTCF/RAD21
E= 1.4e-1040
CTCFnotRAD21
E-value = 2.0e-1173
F
CTCF/RAD21
CTCF
RAD21
1K CTCF sites in CH12
CTCFnotRAD21
G
Mnase-H3
ATAC-seq
<130bp
>140bp
SMARCA5
CTCF/RAD21
CTCFnotRAD21
CTCF summit

Figure 5. SMARCA5 is recruited by the N-terminus of CTCF to open chromatin around CTCF binding sites. (A) Heatmaps showing CTCF occupancy (CUT&RUN) and nucleosome positioning (MNase-seq) in Kasumi-1 cells with CAS9-modified degradation of endogenous SMARCA5 protein using a small molecule proteolysis targeting chimera (PROTAC). The Kasumi-1 cells were either not treated with dTAG-47 (0h) or treated for 24 hours (24h, SMRCA5ko, knockout). The heatmaps are centered on CTCF-bound plus motifs mapped by ChIP-seq in Kasumi-1 cells. The CTCF priming nucleosome (CpN) is indicated by black arrows. At the bottom of the heatmap, a schematic representation illustrates the effects of SMARCA5 knockout on CTCF and nucleosome occupancies. **(B)** MNase-seq profile of nucleosome positioning at CTCF-bound motifs in the plus orientation in PROTAC-modified Kasumi-1 cells treated with dTAG-47 for 0 hours (black, wt) and 24 hours (green, SMARCA5ko). **(C)** Heatmaps of SMARCA5 ChIP-seq data across two groups of CTCF binding sites: remaining CTCF sites (56,276) bound by CTCF in both wtCH12 and mutCH12 cells (top panel); 4,958 lost CTCF sites in mutCH12 cells but restored by ectopic expression of FL-CTCF (lower panel). Red arrows indicate the absence of SMARCA5 occupancy at the lost CTCF sites in mutCH12 cells, even when ectopically expressing either the deltaN CTCF variant or BORIS. **(D)** Genome browser view displaying CTCF (red) and RAD21 (pink) ChIP-seq data alongside ATAC-seq data (brown) in wtCH12 cells. CTCF sites either depleted of cohesin (CTCFnotRAD21) or enriched with cohesin (CTCF/RAD21) are indicated by black arrows. **(E)** CTCF motifs identified within CTCFnotRAD21 and CTCF/RAD21 ChIP-seq peaks in wtCH12 cells. **(F)** Heatmap of CTCF (red) and RAD21 (pink) ChIP-seq occupancy at 1,000 CTCF/RAD21 and CTCFnotRAD21 binding sites in wtCH12 cells, centered at the summit of CTCF peaks. **(G)** Heatmap showing MNase-H3 nucleosome positioning, ATAC-seq (with reads <130 bp indicative of CTCF footprint, and nucleosome-sized fragments >140 bp to determine nucleosome positioning), SMARCA5 ChIP-seq at CTCF/RAD21 (black) and CTCFnotRAD21 (green) binding sites in wtCH12 cells. Panel (G) is connected to the data presented in panel **(F)**.

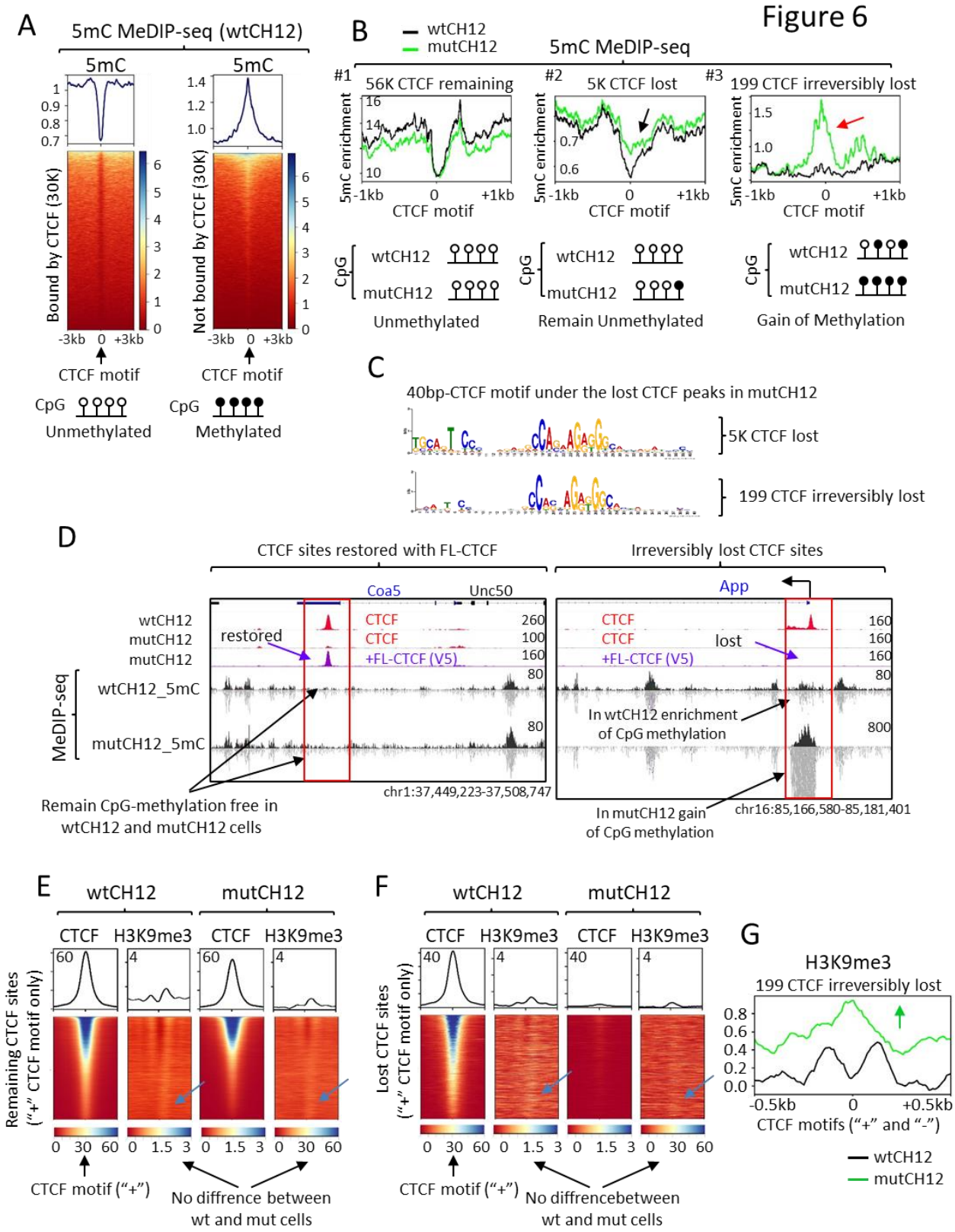
Figure 6
A
5mC MeDIP-seq (wtCH12)
5mC
5mC
Bound by CTCF (30K)
Not bound by CTCF (30K)
-3kb 0 +3kb
CTCF motif
CTCF motif
CpG
Unmethylated
CpG
Methylated
B
wtCH12
mutCH12
5mC MeDIP-seq
#1
56K CTCF remaining
#2
5K CTCF lost
#3
199 CTCF irreversibly lost
5mC enrichment
-1kb 0 +1kb
CTCF motif
CpG
wtCH12
mutCH12
Unmethylated
Remain Unmethylated
Gain of Methylation
C
40bp-CTCF motif under the lost CTCF peaks in mutCH12
5K CTCF lost
199 CTCF irreversibly lost
D
CTCF sites restored with FL-CTCF
Irreversibly lost CTCF sites
Coa5
Unc50
App
wtCH12
mutCH12
mutCH12
restored
CTCF
CTCF
+FL-CTCF (V5)
lost
MeDIP-seq
wtCH12_5mC
mutCH12_5mC
In wtCH12 enrichment of CpG methylation
chr1:37,449,223-37,508,747
chr16:85,166,580-85,181,401
Remain CpG-methylation free in wtCH12 and mutCH12 cells
In mutCH12 gain of CpG methylation
E
wtCH12
mutCH12
CTCF
H3K9me3
Remaining CTCF sites ("+" CTCF motif only)
CTCF motif ("+")
No diffrence between wt and mut cells
F
Lost CTCF sites ("+" CTCF motif only)
No diffrencebetween wt and mut cells
G
H3K9me3
199 CTCF irreversibly lost
-0.5kb 0 +0.5kb
CTCF motifs ("+" and "-")
wtCH12
mutCH12

Figure 6. CTCF occupancy is largely determined by the permissive epigenetic status around its binding sites. (A) Heatmaps showing 5mC MeDIP-seq read alignment centered at CTCF motifs either bound by CTCF (left panel) or not bound by CTCF (right panel) in wtCH12 cells. Below the heatmaps, a schematic representation of CpG methylation status is provided, with open circles indicating unmethylated CpGs and filled black circles representing methylated CpGs, summarizing the data from the corresponding heatmaps. **(B)** Profile of 5mC MeDIP-seq across three groups of CTCF binding sites: (left panel) remaining CTCF sites (56,276) bound by CTCF in both wtCH12 and mutCH12 cells; (middle panel) 4,958 lost CTCF sites (5K) in mutCH12 cells, which are restored by ectopic expression of FL-CTCF; and (right panel) 199 irreversibly lost CTCF sites. Black and red arrows indicate the gain of CpG methylation at the 5K lost CTCF sites and at the irreversibly lost CTCF sites, respectively. A schematic representation of CpG methylation status at the three groups of CTCF sites is shown below the 5mC profiles, highlighting that the irreversibly lost CTCF sites gained CpG methylation (filled black circles) in mutCH12 cells compared to wtCH12 cells. **(C)** The 40-bp MEME-recovered CTCF consensus sequence under the 5K lost CTCF sites compared to the 199 irreversibly lost CTCF sites. **(D)** Genome browser view of CTCF (red) and CTCF-V5 (purple) ChIP-seq data combined with 5mC MeDIP-seq data in wtCH12 cells and mutCH12 cells. The restoration status of CTCF occupancy with ectopic expression of FL-CTCF (V5-Tag antibodies) in mutCH12 cells is indicated by purple arrows. Black arrows show the status of CpG methylation at the lost CTCF sites in wtCH12 versus mutCH12 cells. **(E-F)** Heatmaps of CTCF and H3K9me3 ChIP-seq data in wtCH12 cells versus mutCH12 cells at the remaining CTCF sites (**E**) and the 5k lost CTCF sites (**F**), centered on the CTCF motifs in the plus (sense) orientation of CTCF ChIP-seq peaks. The CTCF priming nucleosome (CpN) is indicated by blue arrows. **(G)** Profile of H3K9me3 ChIP-seq data at the 199 irreversibly lost CTCF sites in wtCH12 cells (black) versus mutCH12 cells (green), centered at CTCF motifs in both orientations, without sorting. The green arrow highlights a gain of H3K9me3 in mutCH12 cells compared to wtCH12 cells.